*DOI:*
10.1016/j.cub.2017.01.069

*Document Version*
Peer reviewed version

## Highlights

- Protein deposits that form during aging associate with the endoplasmic reticulum (ER)
- ER serves as a platform for deposit coalescence during cell fusion
- Farnesylated Hsp40 ($Ydj1^{FS}$) mediates ER-attachment of deposit precursors
- ER diffusion barriers ensure the asymmetric partitioning of $Ydj1^{FS}$ during division

## eTOC Blurb

Saarikangas et al. report that confinement of age-associated protein deposit formation to the aging lineage in yeast involves a two-tiered mechanism. Deposit precursors are captured by ER-membrane-bound chaperone Ydj1. The compartmentalization of the ER by diffusion barriers then facilitates their asymmetric segregation during cell division.

# Confinement of deposit precursors to the yeast aging lineage

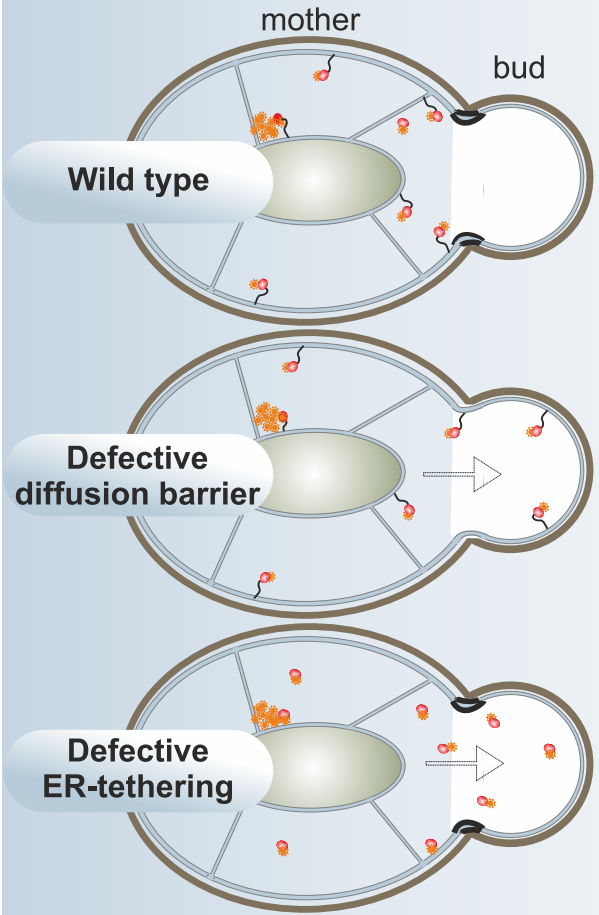


Endoplasmic reticulum (ER)

Farnesylated Ydj1

Non-farnesylated Ydj1

misfolded protein / aggregate seed

ER diffusion barrier

# Compartmentalization of ER-bound chaperone confines protein deposit formation to the aging yeast cell

Juha Saarikangas[1,2], Fabrice Caudron[1,3], Rupali Prasad[1], David F. Moreno[2],

Alessio Bolognesi[1], Martí Aldea[2] and Yves Barral[1]*

[1]ETH Zurich, Institute of Biochemistry, Otto-Stern-Weg 3, 8093 Zurich, Switzerland.

[2]Wissenschaftskolleg zu Berlin, Institute for Advanced Study,

Wallotstraße 19, 14193, Berlin, Germany

[3]Randall Division of Cell and Molecular Biophysics, King's College London,

London SE1 1UL, UK.

[4]Molecular Biology Institute of Barcelona, CSIC. Baldiri i Reixac 15, 08028 Barcelona.

*Lead Contact:

Yves Barral

Tel: +41 44 632 06 78, Fax: +41 44 632 15 91

Email: yves.barral@bc.biol.ethz.ch

**SUMMARY**

In order to produce rejuvenated daughters, dividing budding yeast cells confine aging factors, including protein aggregates, to the aging mother cell. The asymmetric inheritance of these protein deposits is mediated by organelle- and cytoskeletal attachment, and by cell geometry. Yet, it remains unclear how deposit formation is restricted to the aging lineage. Here, we show that selective membrane anchoring and the compartmentalization of the endoplasmic reticulum (ER)-membrane confine protein deposit formation to aging cells during division. Supporting the idea that the age-dependent deposit forms through coalescence of smaller aggregates, two deposits rapidly merged when placed in the same cell by cell-cell fusion. The deposits localized to the ER-membrane, primarily to the nuclear envelope (NE). Strikingly, weakening the diffusion barriers that separate the ER-membrane into mother and bud compartments caused premature formation of deposits in the daughter cells. Detachment of the Hsp40 protein Ydj1 from the ER-membrane elicited a similar phenotype, suggesting that the diffusion barriers and farnesylated Ydj1 functioned together to confine protein deposit formation to mother cells during division. Accordingly, fluorescence correlation spectroscopy measurements in dividing cells indicated that a slow-diffusing, possibly client-bound Ydj1 fraction was asymmetrically enriched in the mother compartment. This asymmetric distribution depended on Ydj1 farnesylation and on intact diffusion barriers. Taken together, we propose that ER-anchored Ydj1 binds deposit precursors and prevents them from spreading into daughter cells during division by subjecting them to the ER diffusion barriers. This ensures that the coalescence of precursors into a single deposit is restricted to the aging lineage.

## INTRODUCTION

The asymmetric partition of specific macromolecules during cell division is key for development, cellular diversity, cell fate determination and aging [1-4]. In stem cells and budding yeast, RNA and protein determinants are asymmetrically inherited during division, modifying gene expression only in the recipient cell [3-5]. Also some cells partition post-translationally modified or damaged macromolecules and organelles unequally between their daughters. This is thought to drive aging of the recipient by negatively influencing its fitness [2,3,6,7]. While the list of unequally partitioned material is expanding, far less is known about the molecular and biophysical mechanisms underlying their asymmetric partition during cell division.

Coalesced protein assemblies represent a diverse class of asymmetrically inherited cell-fate determinants. For example, in budding yeast some coalesced protein assemblies encode epigenetic information [8, 9], while others are associated with cellular dysfunction and linked to aging [2,3,8]. In budding yeast cells, Hsp104-labelled protein aggregates appear as singular deposits during early aging. They are retained in the aging-lineage during division and contribute to aging [10-12]. It is currently unclear 1) why deposits form in aging mother cells, 2) what are their constituents, and, 3) why are they not forming in daughter cells. Rather than resulting from a proteostasis collapse [12], deposits seem to form gradually during early aging, perhaps resulting from slow accumulation of specific misfolded proteins or epigenetic assemblies. If so, the deposits precursors might also need to be confined to the aging mother cell, in order to prevent their passage and coalescence in the bud. Here, we sought to investigate the mechanisms that restrict the deposit formation to the aging mother cells.

## RESULTS

In order to understand where coalescence might take place in the aging mother cells of *Saccharomyces cerevisiae*, we imaged 3-6 generation old cells co-expressing Hsp104-

mCherry together with GFP-tagged markers for the endoplasmic reticulum (ER; Sec61 and Sec71; Fig. 1A and S1B), nucleus (Pre6; Fig. S1C), vacuole (Yml018c; Fig. S1D) mitochondria (Tom70; Fig. S1E), peroxisomes (Pex3; Fig. S1F), spindle pole bodies (SPBs, centrosome equivalents; Spc72; Fig. S1G), and characterized the localization of the age-associated deposit relative to these organelles. Strikingly, the deposit (bright Hsp104-labelled dot) [12] was always apposed to the ER membrane, typically at the nuclear envelope (NE) (Fig. 1A-B, S1A-B). However, the deposits did not colocalize with SPBs (Fig. 1B, Fig S1G), unlike aggresomes in mammalian cells [13]. Approximately 60% and 40% of them also touched vacuolar and mitochondrial membranes, respectively (Fig. 1B). These results are consistent with different protein inclusions associating with specific organelles during division [14-18].

Live-cell imaging confirmed that ER extensions, generally emanating from the nuclear envelope, encapsulated the age-associated deposit (Fig. 1C). The localization of the Hsp104-labelled deposit relative to ER (Sec71-GFP), vacuole (Ym018c) and mitochondrial markers was imaged every ten minutes over 100 minutes and quantified as cells progressed through a full division cycle (N=15, Fig. S2A-C). At each time point, the frequency of apposition to the ER varied between 93 and 100% over the duration of the movie. The average frequency of apposition to the vacuole and mitochondria were consistently lower (33-66%, and to 33-60% respectively; Fig. 1D). Accordingly, in time-lapse movies of mating cells (Fig. 1E) age-associated deposits followed the movements of the ER (Fig. 1F), but not of the vacuole (Fig. 1G-H). We concluded that the age-associated deposit was tethered to the ER membrane and transiently contacted vacuoles and mitochondria. In contrast, heat stress-induced inclusions favor inter-organelle (ER-mitochondrion) contact sites [14].

Structured illumination microscopy of cells co-expressing the ER marker Sec71-GFP and Hsp104-mCherry validated that age-associated deposits were apposed to the ER, typically at the nuclear rim (96% of cases; Fig. 1I) and occasionally inside the nucleus (38%, N=26 cells;

Fig. 1J). This intranuclear localization is reminiscent of the intranuclear quality control compartment (INQ) [19], despite the INQ marker Btn2 not co-localizing with the age-associated deposit [12]. The exact structural and functional relationships between the Hsp104 structures that arise during aging and INQ/JUNQ deposits remain to be determined [12,15,19]. Collectively, our data establish that age-associated deposits are tethered to the ER membranes.

**Age-associated deposits tend to merge**

Limiting the deposits number facilitates their asymmetric partition between daughters during cell division [20,21]. During budding yeast aging, states of two or more Hsp104-foci are rare and unstable [12], typically reverting to a single deposit state (Fig. 2A), suggesting that large deposits form through merger of smaller entities over time. However, due to the small size of these entities, such events have not been visualized with conventional microscopy. To investigate whether merger could underlie the deposits' singularity, we tested the consequence of introducing two deposits into the same cell. Hence, haploid cells of opposite mating types, expressing either Hsp104-GFP or Hsp104-mCherry, were mixed, and fusing partners each containing one visible deposit (Fig. 2B), were monitored (Fig. 2B-C). As expected, the cytoplasmic Hsp104-GFP and Hsp104-mCherry signals mixed homogeneously immediately after cell fusion (Fig. 2D, Movie S1). However, the signal at the deposit typically remained initially in its original color (green or red; Fig. 2D, Movie S1), consistent with deposit-associated Hsp104 exchanging slowly [12]. Remarkably, the majority of the original deposits (82%, N=82 cell pairs) merged together into a single deposit, which remained in the zygote throughout its subsequent budding cycles (Fig. 2E-G, Fig. S3A-B, Movie S1). Thus, fusion of coexisting deposits ensured their singularity, at least upon mating.

**Merging of deposits requires a continuous ER membrane**

Homozygous *prm3Δ/prm3*Δ mutant zygotes are defective in fusing the ER and NE of the partner cells upon mating [22] (Fig. 2H). We reasoned that this should impede the merger of

ER-tethered deposits. Accodingly, we observed that prior to their first division most homozygous *prm3Δ/prm3*Δ mutant zygotes (81%) failed to merge their deposits (Fig. 2I-L; p<0.001; N=42-82). Beyond confirming that the deposits localize to the ER surface, this observation indicate 1) that the deposit is in a 'coalescent state' and can grow through coalescence of precursor structures, and 2).that the ER-membrane serves as a platform for coalescence.

**Compartmentalization of the ER membrane helps confining deposit formation into the mother cells**

Lateral diffusion barriers compartmentalize the ER-membrane at the future division plane of dividing yeast, mouse neural stem cells and embryos of *C. elegans* [23-28]. To test if the diffusion barriers help retaining the age-associated protein deposits into yeast mother cells, we harvested aged cells (~10-14 generations) [29] and measured the frequencies at which deposits passed to the daughter cell upon division. Passage was observed in <2% of wild type cells (Fig. 3A-B). Weakening of the diffusion barrier at the cortical ER (cER; *bud1Δ*) [23] or at both the cER and the outer nuclear membrane (ONM; *sur2Δ*) [28] did not significantly promote passage of deposits into the bud (WT: 1,3%; *bud1Δ:* 1,7%, *sur2Δ:* 2,8%, n.s.). Deletion of *BUD6*, which is required for integrity of both the cER and ONM barriers [24] and for actin cable assembly [30], increased 5 folds the passage frequency of deposits into the bud (Fig. 3A-B; 10,2%; p<0.05), without changing their number (Fig. S3). We conclude that the decreased retention of the deposits into the *bud6*Δ mutant mother cells is due to actin cable defects, consistently with actin cables promoting the partition of protein inclusions [31]. Together, our data indicate that age-dependent deposits do not need the diffusion barriers at the bud neck for their retention in the aging lineage upon cell division.

However, all barrier-defective strains shared a remarkable phenotype: the daughter cells of aged *bud1Δ, sur2Δ* and *bud6Δ* mutant cells formed a deposit >3 times faster than wild type daughter cells (daughter cells forming deposit during their first cell cycle: 38%, p<0.01; 40%,

p<0.05; 45%, p<0.01; and 11%, respectively; Fig. 3A,C). Thus, although retention of assembled age-dependent deposits did not depend on diffusion barriers**,** the barrier was required to confine the deposit formation to the aging lineage. Furthermore, since the *sur2*Δ mutant cells did not show a stronger phenotype than the *bud1*Δ mutant cells, the confinement depended mainly on the cER barrier.

**Confinement of deposit precursors to the mother cell requires Ydj1 tethering to ER-membranes**

One possible mechanism by which the ER barrier could confine deposit formation to the mother cell would be if proteins targeted to deposits were anchored to the cytoplasmic side of the ER-membrane prior to coalescing into the deposit. Thus we searched for ER-bound chaperones that could contribute to membrane anchorage. Among the factors associating with age-associated deposits [12], only the J-domain protein Ydj1 is known to associate with the ER-membrane. Post-translational covalent linkage of a farnesyl moiety in the C-terminus of Ydj1 drives its ER-anchorage [32]. Ydj1 co-operates with Hsp104 and Hsp70 chaperones to re-solubilize misfolded proteins [33,34]. Imaging of cells expressing N-terminally tagged GFP-Ydj1, which harbors a functional farnesylation motif (FS), showed that 9.4% of the Hsp104-labelled deposits (Hsp104-mCherry) were enriched in Ydj1 (Fig. S5A). The *ydj1*Δ mutant cells grow slowly, form large dysmorphic cells with elongated buds and display fragmented Hsp104 foci throughout mother and bud (Fig. S5B-C) [35]. These phenotypes reflect the roles of Ydj1 in protein solubilization and degradation [33,34], but also indicated that it might help restricting deposit formation to the mother cell.

Thus, we investigated whether interaction of Ydj1 with the ER-membrane helped confining deposit formation into the mother cell. Mutating the cysteine 406 to serine abrogates Ydj1 farnesylation, and renders the cells heat sensitive but does not abrogate Ydj1 function in protein folding [32]. Time-lapse imaging of Hsp104-GFP indicated that the daughters of *YDJ1-C406S* mutant cells formed a deposit >6 fold faster than wild type daughter cells (Fig.

4A-B,D). Subsequently, these cells efficiently retained this deposit (frequency of passage into the bud: 0.7% in WT, vs. 1.5% in *YDJ1-C406S*; n.s; Fig. 4A-C), which still remained associated to the ER-membrane (co-localization with Sec71: WT 99.5%, Ydj1C406S 99.5%, Fig. S5D-F). Thus, detaching Ydj1 from the ER specifically expedites the deposit formation in the bud, whereas ER association and mother-retention of the deposits is facilitated by other factors.

In order to understand how Ydj1 function relates to that of the barrier in the cER, we first tested whether the Ydj1-C406S-mutation affected barrier formation. We assayed barrier strength using fluorescent loss in photobleaching (FLIP) [28,36] and the ER-membrane protein Sec71 as a reporter (Fig. S5G-K). No barrier decrease was observed in the *YDJ1-C406S* mutant cells (Barrier Index: WT: 5,4±0.7; Ydj1C406S: 6.5±0.8; Fig. S5K). Furthermore, we noted that the daughter cells of *YDJ1-C406S sur2Δ* (65.4%), *YDJ1-C406S bud1Δ* (67.7%) and *YDJ1-C406S bud6Δ* (78.7%) double mutant cells formed deposits as frequently as those of the *YDJ1-C406S* single mutant cells (69.8%; n.s.; Fig. 4E,F). Thus, the diffusion barriers and ER-tethering of Ydj1 function jointly in confining deposit formation to the mother cell.

**The diffusion barrier facilitates the asymmetric retention of slow-diffusing Ydj1$^{FS}$ into the mother cells during mitosis**

The results above suggested that farnesylated Ydj1 acted as a membrane anchor for proteins destined to the age-dependent deposit, thereby subjecting them to compartmentalization by the lateral diffusion barriers and preventing their transmission to daughter cells. In order to test this idea, we next compared the diffusion dynamics of Ydj1 in mother and bud compartments, using fluorescence correlation spectroscopy (FCS; Fig. 5A). Since the diffusion rate of a protein reflects the size of the particle and the environment in which it diffuses, increased association of Ydj1 with clients in the mother cell should slow down its diffusion. However, such effects could be compounded by the degree of membrane

association of Ydj1 in one compartment versus the other. Thus, we generated two chromosomally inserted constructs: one allowing Ydj1 to be farnesylated (Ydj1-GFP$^{FS}$), and a similar construct lacking the farnesylation site (C406S, Ydj1-GFP$^{C406S}$). Importantly, analysis of wild type mother-bud pairs revealed that Ydj1-GFP$^{FS}$ diffused on average significantly slower in the mother than in the bud compartment (D=3.86±0.059 vs. 4.53±0.073; p<0.0001; Fig. 5B). In contrast, Ydj1-GFP$^{C406S}$ diffused significantly faster both in the mother and the bud (Ydj1-GFP$^{C406S}$ D=5.34±0.147 and 5.48±0.149; Fig. 5B), consistent with the protein being detached from the membrane. Furthermore, its speed was similar in both compartments (Ydj1-GFP$^{C406S}$ Mother$^{D}$ vs. Bud$^{D}$ n.s). In the barrier defective *sur2*Δ mutant cells, Ydj1$^{FS}$ diffused nearly as fast in the mother and in the bud (3.91±0.066 vs 4.15±0.084, p<0.05; Fig. 5B). Importantly, the diffusion of Ydj1$^{FS}$ was significantly slower in the *sur2Δ*mutant than in wild type buds (Bud$^{D}$ in wild type vs. *sur2Δ*p<0.005), whereas diffusion in the mother compartment was not significantly affected. Analysis of the diffusion profiles in single mother-bud pairs indicated that cytosolic GFP alone diffused at a similar speed in both the mother and bud compartments (GFP Mother$^{D}$/Bud$^{D}$=1.01±0.03), whereas the diffusion of Ydj1-GFP$^{FS}$ was asymmetric, being on average ~12% slower in the mother than in the bud compartment (Fig. 5C; Ydj1-GFP$^{FS}$ Mother$^{D}$/Bud$^{D}$=0.88±0.02; GFP vs. Ydj1-GFP$^{FS}$, p<0.005). Importantly, both the C406S mutation and barrier inactivation abolished this asymmetry (Fig. 5C; Ydj1-GFP$^{C406S}$ Mother$^{D}$/Bud$^{D}$=1.01±0.04; Ydj1-GFP$^{FS}$ vs. Ydj1-GFP$^{C406S}$ p<0.005; *sur2Δ* Mother$^{D}$/Bud$^{D}$=0.970.02; wild type vs. *sur2Δ* p<0.005). Thus, Ydj1 diffused slower in the mother than in her bud; this difference required its farnesylation and intact diffusion barriers.

The slower diffusion of Ydj1-GFP$^{FS}$ in mother versus bud compartments might reflect the protein being more frequently farnesylated and tethered to the membrane in mother cells, and/or being more frequently associated with clients or other factors. The average diffusion speed of GFP (21.22±0.09) was 4.7 times faster than the non-membrane bound Ydj1-GFP$^{C406S}$ (4.52±0.09), at similar molecular brightness (GFP 5.54±0.26; Ydj1-GFP$^{C406S}$

7.46±0.21). If only their own size affected their diffusion, Ydj1-GFP$^{C406S}$ should be only 1.34 fold slower than GFP alone. Hence, cargo binding seems to slow down Ydj1$^{C406S}$ diffusion in vivo.

Next, we asked whether increased detachment of Ydj1 from the ER-membrane caused its accelerated diffusion in the bud (Fig. 5B). Molecules freely diffusing in a continuous aqueous phase (cytoplasm or ER lumen) exchange nearly instantly between mother and bud and, thus, in FLIP assays (fluorescence loss in photobleaching) their fluorescence decays at similar speeds in both compartments [23,37]. Upon continuously photobleaching a small area in the mother cell [28,36], the fluorescence of GFP-Ydj1 (intact farnesylation motif in the C-terminus) decayed 6 times slower in the bud than in the mother compartment (Figure 5D-F). In contrast, the fluorescence of the Ydj1-GFP protein (non-farnesylated and cytoplasmic) decayed nearly as fast in the bud as in the mother compartments (Fig. 5E-F; barrier index GFP-Ydj1: 5.96±0.45, Ydj1-GFP 1.62±0.01; $p<0.001$). Thus, the farnesylated species of Ydj1 do not exchange rapidly between bud and mother, excluding the possibility that they are cytoplasmic in the bud. We conclude that Ydj1 compartmentalization requires its farnesylation, and that Ydj1 is anchored to the ER-membrane in both mother and bud compartments. Thus, increased cargo-binding in the mother cell likely underlies the slower diffusion of Ydj1 in that compartment.

Comparing FLIP traces between wild type and *sur2*Δ mutant cells indicated that GFP-Ydj1 exchanged approximately 30% faster between mother and bud upon barrier inactivation (Figure 5F; barrier index WT: 5.96±0.45, *sur2Δ*: 4.16±0.31; $p<0.01$). We conclude that the diffusion barrier helps compartmentalizing the cargo-bound, slow diffusing Ydj1 to the mother cell during division.

**Ydj1-mediated membrane confinement suppresses the prion phenotype of Sup35**

In order to gain insights into the possible relevance of Ydj1 confinement, we sought to test how ER-tethering of Ydj1 affects one of its known clients. The translation termination factor Sup35 accumulates in the age-associated Hsp104-deposit of [*PSI*+] but not of [psi-] cells, i.e., only when it is converted into its amyloid-forming prion form [12]. Thus, prion-converted Sup35 is a potential client of Ydj1 during aging. Supporting this notion, Ydj1 physically associates with Sup35 [38] and its over-expression cures the [*PSI*+] prion-state [39]. Importantly, diffusion of Sup35 aggregation oligomers (propagons) into buds ensures the heritability of the [*PSI*+] prion state. The number of Sup35 propagons determines the strength of the [*PSI*+] phenotype: strong variants show large numbers of small, cytosolic oligomers that propagate the prion phenotype and convert the functional soluble Sup35 (inactivating its translation termination activity) more robustly than weak variants, which contain larger Sup35 aggregates and smaller number of converting and propagating species (see e.g., [40,41]. Thus, [*PSI*+] strength is a proxy for the spreading of Sup35 propagons in the population. Therefore, we quantified this strength by expressing an mRNA carrying the GFP coding sequence interrupted by a premature stop codon. In [*psi*-] strains, translation termination at the stop prevents GFP expression (see Fig. 5G), whereas increased read-through in the [*PSI*+] allows GFP accumulation. The degree of this accumulation depends on prion strength [41]. Using flow cytometry, we assayed how mutating the farnesylation site (*YDJ1-C406S*) or the peptide-binding pocket of Ydj1 (*YDJ1-L135S* - hampering protein folding but not in prion-binding [46]) affected stop codon read-through in [*PSI*+] and [*psi*-] cells (Fig. 5G). As reported [41], GFP fluorescence was increased >6 fold in the [*PSI*+] strain expressing wild type *YDJ1* compared to the [*psi*-] strain (Fig. 5F; [*PSI*+]: 10273 AU±1074; [*psi*-]: 1523 AU±11). In comparison, the [*PSI*+] cells expressing Ydj1-C406S displayed an additional >2-fold increase in GFP expression (Fig. 5F; 22218 AU±2461, $p<0.01$). In contrast, the peptide-binding mutant did not potentiate the [*PSI*+] phenotype (Fig. 5F; L135S: 7923 AU±129) [38]. Taken together, these results indicate that farnesylated Ydj1, and not Ydj1 function in protein folding, suppresses the number of Sup35 propagons in the population. We

propose that this effect is due to loading of Sup35 oligomers to ER-bound Ydj1 to limit their propagation from aging mothers to their buds.

## DISCUSSION

Organismal aging is associated with proteome changes, including the appearance of protein deposits [42]. In replicative aged budding yeast cells, microscopically visible protein deposits appear during early aging, yet their appearance does not seem to be caused by proteostasis collapse [12]. Their origin in the aging lineage remains therefore unclear. We found that age-associated protein deposits have the propensity to merge (Fig. 2; [12]), suggesting that they are build over time through fusion of smaller, microscopically invisible precursors. Since the deposits do not form in the growing bud, these small precursors must be somehow confined into the mother cells prior to their solubilization, degradation or incorporation into the large deposits, and not passed on during mitosis.

Here we propose a framework to explain how deposit formation is confined to the aging lineage. Age-associated deposits are tethered to the ER membrane. This continuous membrane is laterally compartmentalized at the future cell division plane by diffusion barriers [23,24,28]. Both disruption of ER compartmentalization and detachment of the ER-anchored DnaJ protein, Ydj1, accelerated deposit appearance in the daughter cells, suggesting that deposit constituents might enter the buds more frequently in these mutants. Molecule measurements established that Ydj1 diffused significantly slower in the mother than in the bud (Fig. 5) and that abrogating the barrier or detaching Ydj1 from the ER-membrane erased this difference and accelerated deposit formation in daughter cells. Based on this, we suggest that Ydj1 is more frequently associated with client proteins and macrocomplexes in the mother cell than in her bud (Fig. 5). Although unequivocal demonstration of Ydj1 client-binding will require additional work, our results provide a plausible mechanistic explanation for how protein deposit formation is confined in a lineage-specific manner. We propose that capturing of deposit precursors to the ER membrane by Ydj1, and the impeded diffusion of

such species from the mother into the bud by the diffusion barriers together ensure that the coalescence of precursors into a larger deposit takes place primarily in the aging mother cell.

Alternatively, all of these mutants could accelerate deposit formation by increasing the rate of protein misfolding. However, we find this alternative unlikely because neither the barrier mutant cells nor cells expressing non-farnesylated Ydj1 displayed noticeable reduction of Ydj1 diffusion. Thus, it is unlikely that they accumulate more unfolded proteins. Furthermore, the *YDJ1-C406S* mutation and all barrier defects accelerated deposit formation through the same mechanism, which is therefore unlikely to rely on increased protein-misfolding. Finally, while the membrane-detached version of Ydj1 increased Sup35 prion strength, which reflects an increased number of spreading propagons, this effect was not recapitulated by the Ydj1 mutant that impaired protein folding. From these lines of evidence, we conclude that increased deposit formation in the daughter cells of diffusion barrier defective or membrane-detached Ydj1 mutant cells is caused by defective confinement of aggregate precursors rather than increased protein misfolding.

It is unknown why protein deposits form with age and what they are constituted of. We suggest that the formation of deposits during aging might be associated with the gradual accumulation of deposit precursors in the mother cells. It is possible that the progressive accumulation of such species may overwhelm the capturing system over time. Furthermore, the deposits may then themselves become a source of propagating seeds, as the disaggregation machinery attempts to dissociate them. Indeed, we found that the deposit formation frequencies in daughter cells correlated with the deposit status of mother cells. In wild type and *sur2*Δ mutant cells, the daughters born from mothers with pre-existing deposit formed a deposit more frequently during their first cycle than daughter cells born from a mother that neither contained a deposit nor formed one immediately after division (9.0%±3.2 vs 2.8%±2 in WT and 33.8%±6.8 vs 1.9%±1.9 in the *sur2Δ* mutant cells, respectively). Thus, the formation of visible deposits over time takes place through diffusion barrier mediated

confinement of deposit precursors. Furthermore, the growing deposits of aged cells may lead to increased seeding of deposit precursors.

From yeast to mammals, aggregation prone protein sequences, such as intrinsically disordered and prion-like domains, have been associated with the formation of phase-separated protein assemblies involved in many processes, including epigenetic and adaptive regulations and the compartmentalization of biochemical reactions [8,43]. The dynamics of these stoichiometrically ambiguous assemblies are governed by their material state which can vary from liquid-like to less-dynamic hydrogels and solids [44]. Such assembly mechanisms may require particularly high maintenance and could be vulnerable to transit into aberrant states of aggregation [43,45]. Therefore, it is now very timely to identify the mechanisms that prevent the uncontrolled formation and spreading of different aggregation oligomers. Indeed, such uncontrolled spreading is particularly linked to age-associated neurodegenerative conditions in humans [46], such as ALS, Alzheimer's, Parkinson's and Huntington's diseases. There, the spread of aggregating species and the mode of their aggregation are potentially key features in aggregation-induced pathogenicity [46,47]. Thus, spatial confinement and collection of aggregating oligomers into larger deposits potentially protects the cell against their toxicity. It is noteworthy that human DnaJ-proteins have been found to be key regulators of aggregating proteins in various proteopathic diseases, and that mutations in genes encoding DnaJ proteins can predispose to certain aggregation diseases [48]. Thus, Ydj1 and its human homologues are key coordinators of aging- and disease-associated protein aggregation.

Intriguingly, the confinement of aggregate precursors shows similarities with the confinement of extra-chromosomal DNA circles (ERCs) into yeast mother cells [6,24,49]. Mediated by the SAGA complex, ERCs bind to a subset [49] of nuclear pore complexes, facilitating their retention by the diffusion barrier at the bud neck [24,49]. Therefore, we propose that selective anchorage to the ER-membrane together with membrane compartmentalization by

diffusion barriers represent a general theme to promote the asymmetric partitioning of diverse fate determinants during asymmetric cell division. This concept may be wide spread, since diffusion barriers confine other membranes as well [50], for example the plasma membrane at the base of primary cilia [51] and dendritic spines [52]. Our finding that post-translational lipidation can prevent proteins from passing diffusion barriers may therefore explain how certain cytoplasmic proteins can be enriched to specific regions of the cell to carry out compartment-specific tasks.

## EXPERIMENTAL PROCEDURES

### Microscopy

All images (except the Figs. 1G-H, S5C,E) were acquired at 30°C with a DeltaVision microscope (GE Healthcare / Applied Precision) equiped with 100X/1.40 and 60x/1.42 NA Olympus objectives, 250W Xenon lamps and a coolSNAP CCD HQ2 camera. Imaging was performed with the indicated time intervals by obtaining 9-15 z-sections for each time point. Images were deconvolved with Softworx (Applied Precision) and maximum projected unless otherwise indicated.

Structured illumination microscopy was performed with Applied Precision OMX Blaze (GE Healthcare) microscope, using a 60X 1.42 NA Plan Apo oil objective and sCMOS OMX V4 camera. Imaging was performed with immersion oil (refractive index 1.516), using 488 and 568 nm lasers and 528/35 and 609/37 nm emission filters. Total depth of 1.25 µm; one focal plane every 150 nm. Image reconstruction was performed using Softworx with a Wiener filter of 0.002.

FLIP experiments were performed as described [43,46] on an LSM 780 (Carl Zeiss, Jena, Germany) confocal microscope with a 63x/1.4 NA objective and a multiarray 32PMT GaAsP detector, using 3.5% (Sec71), and 12% (GFP-Ydj1) of 488nm argon laser intensity. Bleaching was applied with 100 iterations at 100% laser power over a period of 50 frames. The strains are listed in Supplemental Table and the growth conditions, image analyses,

fluorescence correlation spectroscopy and flow cytometry experiments are described in Supplemental Experimental Procedures.

**Statistical analyses**

All the statistical analyses were performed and the graphs prepared with PRISM5 software (Graphpad Software Inc.). Comparisons between two groups were done with t-test and multiple groups with one-way ANOVA, using Dunnet's or Newman-Keuls post-tests. In the text, '±' values indicate standard error of mean.

**Author contributions**

J.S., F.C. and Y.B. conceived the study. J.S., F.C., R.P., D.M., A.B., and M.A. performed experiments and analyzed the data. J.S. and Y.B. wrote the manuscript with input from all the authors.

**Acknowledgements**

This study is supported by FEBS and the Finnish Cultural Foundation (J.S.) and European Research Council and the ETH Zurich (J.S., F.C., R.P., A.B., Y.B.). We are grateful to Maya Schuldiner, Tricia Serio, Simon Alberti, and to Douglas Cyr for kindly providing strains and plasmids. ETH Zurich Scientific Center for Optical and Electron Microscopy (ScopeM) and the Flow Cytometry core facilities are acknowledged for instrumentation and technical support. We thank Anne Meinema for providing computational tools and Haochen Yu for giving valuable feedback on the manuscript.

**REFERENCES**

1. Mortimer, R.K., and Johnston, J.R. (1959). Life span of individual yeast cells. Nature *183*, 1751-1752.
2. Denoth Lippuner, A., Julou, T., and Barral, Y. (2014). Budding yeast as a model organism to study the effects of age. FEMS microbiology reviews *38*, 300-325.
3. Higuchi-Sanabria, R., Pernice, W.M., Vevea, J.D., Alessi Wolken, D.M., Boldogh, I.R., and Pon, L.A. (2014). Role of asymmetric cell division in lifespan control in Saccharomyces cerevisiae. FEMS yeast research.

4. Neumuller, R.A., and Knoblich, J.A. (2009). Dividing cellular asymmetry: asymmetric cell division and its implications for stem cells and cancer. Genes & development *23*, 2675-2699.
5. Singer-Kruger, B., and Jansen, R.P. (2014). Here, there, everywhere. mRNA localization in budding yeast. RNA Biol *11*, 1031-1039.
6. Ouellet, J., and Barral, Y. (2012). Organelle segregation during mitosis: lessons from asymmetrically dividing cells. The Journal of cell biology *196*, 305-313.
7. Liu, L., and Rando, T.A. (2011). Manifestations and mechanisms of stem cell aging. The Journal of cell biology *193*, 257-266.
8. Saarikangas, J., and Barral, Y. (2016). Protein aggregation as a mechanism of adaptive cellular responses. Current genetics.
9. Caudron, F., and Barral, Y. (2013). A super-assembly of Whi3 encodes memory of deceptive encounters by single cells during yeast courtship. Cell *155*, 1244-1257.
10. Aguilaniu, H., Gustafsson, L., Rigoulet, M., and Nystrom, T. (2003). Asymmetric inheritance of oxidatively damaged proteins during cytokinesis. Science *299*, 1751-1753.
11. Erjavec, N., Larsson, L., Grantham, J., and Nystrom, T. (2007). Accelerated aging and failure to segregate damaged proteins in Sir2 mutants can be suppressed by overproducing the protein aggregation-remodeling factor Hsp104p. Genes & development *21*, 2410-2421.
12. Saarikangas, J., and Barral, Y. (2015). Protein aggregates are associated with replicative aging without compromising protein quality control. eLife *4*.
13. Johnston, J.A., Ward, C.L., and Kopito, R.R. (1998). Aggresomes: a cellular response to misfolded proteins. The Journal of cell biology *143*, 1883-1898.
14. Zhou, C., Slaughter, B.D., Unruh, J.R., Guo, F., Yu, Z., Mickey, K., Narkar, A., Ross, R.T., McClain, M., and Li, R. (2014). Organelle-based aggregation and retention of damaged proteins in asymmetrically dividing cells. Cell *159*, 530-542.
15. Kaganovich, D., Kopito, R., and Frydman, J. (2008). Misfolded proteins partition between two distinct quality control compartments. Nature *454*, 1088-1095.
16. Spokoini, R., Moldavski, O., Nahmias, Y., England, J.L., Schuldiner, M., and Kaganovich, D. (2012). Confinement to organelle-associated inclusion structures mediates asymmetric inheritance of aggregated protein in budding yeast. Cell reports *2*, 738-747.
17. Escusa-Toret, S., Vonk, W.I., and Frydman, J. (2013). Spatial sequestration of misfolded proteins by a dynamic chaperone pathway enhances cellular fitness during stress. Nature cell biology *15*, 1231-1243.
18. Hill, S.M., Hao, X., Gronvall, J., Spikings-Nordby, S., Widlund, P.O., Amen, T., Jorhov, A., Josefson, R., Kaganovich, D., Liu, B., et al. (2016). Asymmetric Inheritance of Aggregated Proteins and Age Reset in Yeast Are Regulated by Vac17-Dependent Vacuolar Functions. Cell reports *16*, 826-838.
19. Miller, S.B., Ho, C.T., Winkler, J., Khokhrina, M., Neuner, A., Mohamed, M.Y., Guilbride, D.L., Richter, K., Lisby, M., Schiebel, E., et al. (2015). Compartment-specific aggregases direct distinct nuclear and cytoplasmic aggregate deposition. The EMBO journal *34*, 778-797.
20. Coelho, M., Lade, S.J., Alberti, S., Gross, T., and Tolic, I.M. (2014). Fusion of protein aggregates facilitates asymmetric damage segregation. PLoS biology *12*, e1001886.
21. Lade, S.J., Coelho, M., Tolic, I.M., and Gross, T. (2015). Fusion leads to effective segregation of damage during cell division: An analytical treatment. J Theor Biol *378*, 47-55.
22. Melloy, P., Shen, S., White, E., and Rose, M.D. (2009). Distinct roles for key karyogamy proteins during yeast nuclear fusion. Molecular biology of the cell *20*, 3773-3782.
23. Luedeke, C., Frei, S.B., Sbalzarini, I., Schwarz, H., Spang, A., and Barral, Y. (2005). Septin-dependent compartmentalization of the endoplasmic reticulum during yeast polarized growth. The Journal of cell biology *169*, 897-908.

24. Shcheprova, Z., Baldi, S., Frei, S.B., Gonnet, G., and Barral, Y. (2008). A mechanism for asymmetric segregation of age during yeast budding. Nature *454*, 728-734.
25. Chao, J.T., Wong, A.K., Tavassoli, S., Young, B.P., Chruscicki, A., Fang, N.N., Howe, L.J., Mayor, T., Foster, L.J., and Loewen, C.J. (2014). Polarization of the endoplasmic reticulum by ER-septin tethering. Cell *158*, 620-632.
26. Lee, Z.Y., Prouteau, M., Gotta, M., and Barral, Y. (2016). Compartmentalization of the endoplasmic reticulum in the early C. elegans embryos. The Journal of cell biology *214*, 665-676.
27. Moore, D.L., Pilz, G.A., Arauzo-Bravo, M.J., Barral, Y., and Jessberger, S. (2015). A mechanism for the segregation of age in mammalian neural stem cells. Science *349*, 1334-1338.
28. Clay, L., Caudron, F., Denoth-Lippuner, A., Boettcher, B., Buvelot Frei, S., Snapp, E.L., and Barral, Y. (2014). A sphingolipid-dependent diffusion barrier confines ER stress to the yeast mother cell. eLife *3*, e01883.
29. Lindstrom, D.L., and Gottschling, D.E. (2009). The mother enrichment program: a genetic system for facile replicative life span analysis in Saccharomyces cerevisiae. Genetics *183*, 413-422, 411SI-413SI.
30. Moseley, J.B., and Goode, B.L. (2005). Differential activities and regulation of Saccharomyces cerevisiae formin proteins Bni1 and Bnr1 by Bud6. J Biol Chem *280*, 28023-28033.
31. Liu, B., Larsson, L., Caballero, A., Hao, X., Oling, D., Grantham, J., and Nystrom, T. (2010). The polarisome is required for segregation and retrograde transport of protein aggregates. Cell *140*, 257-267.
32. Caplan, A.J., Tsai, J., Casey, P.J., and Douglas, M.G. (1992). Farnesylation of YDJ1p is required for function at elevated growth temperatures in Saccharomyces cerevisiae. J Biol Chem *267*, 18890-18895.
33. Cyr, D.M. (1995). Cooperation of the molecular chaperone Ydj1 with specific Hsp70 homologs to suppress protein aggregation. FEBS Lett *359*, 129-132.
34. Glover, J.R., and Lindquist, S. (1998). Hsp104, Hsp70, and Hsp40: a novel chaperone system that rescues previously aggregated proteins. Cell *94*, 73-82.
35. Hill, S.M., Hao, X., Liu, B., and Nystrom, T. (2014). Life-span extension by a metacaspase in the yeast Saccharomyces cerevisiae. Science *344*, 1389-1392.
36. Bolognesi, A., Sliwa-Gonzalez, A., Prasad, R., and Barral, Y. (2016). Fluorescence Recovery After Photo-Bleaching (FRAP) and Fluorescence Loss in Photo-Bleaching (FLIP) Experiments to Study Protein Dynamics During Budding Yeast Cell Division. Methods Mol Biol *1369*, 25-44.
37. Dobbelaere, J., and Barral, Y. (2004). Spatial coordination of cytokinetic events by compartmentalization of the cell cortex. Science *305*, 393-396.
38. Summers, D.W., Douglas, P.M., Ren, H.Y., and Cyr, D.M. (2009). The type I Hsp40 Ydj1 utilizes a farnesyl moiety and zinc finger-like region to suppress prion toxicity. J Biol Chem *284*, 3628-3639.
39. Kushnirov, V.V., Kryndushkin, D.S., Boguta, M., Smirnov, V.N., and Ter-Avanesyan, M.D. (2000). Chaperones that cure yeast artificial [PSI+] and their prion-specific effects. Current biology : CB *10*, 1443-1446.
40. Tanaka, M., Collins, S.R., Toyama, B.H., and Weissman, J.S. (2006). The physical basis of how prion conformations determine strain phenotypes. Nature *442*, 585-589.
41. Derdowski, A., Sindi, S.S., Klaips, C.L., DiSalvo, S., and Serio, T.R. (2010). A size threshold limits prion transmission and establishes phenotypic diversity. Science *330*, 680-683.
42. Vilchez, D., Saez, I., and Dillin, A. (2014). The role of protein clearance mechanisms in organismal ageing and age-related diseases. Nature communications *5*, 5659.
43. March, Z.M., King, O.D., and Shorter, J. (2016). Prion-like domains as epigenetic regulators, scaffolds for subcellular organization, and drivers of neurodegenerative disease. Brain Res *1647*, 9-18.

44. Hyman, A.A., Weber, C.A., and Julicher, F. (2014). Liquid-liquid phase separation in biology. Annual review of cell and developmental biology *30*, 39-58.
45. Alberti, S., and Hyman, A.A. (2016). Are aberrant phase transitions a driver of cellular aging? Bioessays *38*, 959-968.
46. Polymenidou, M., and Cleveland, D.W. (2012). Prion-like spread of protein aggregates in neurodegeneration. J Exp Med *209*, 889-893.
47. Tyedmers, J., Mogk, A., and Bukau, B. (2010). Cellular strategies for controlling protein aggregation. Nature reviews. Molecular cell biology *11*, 777-788.
48. Kakkar, V., Prins, L.C., and Kampinga, H.H. (2012). DNAJ proteins and protein aggregation diseases. Curr Top Med Chem *12*, 2479-2490.
49. Denoth-Lippuner, A., Krzyzanowski, M.K., Stober, C., and Barral, Y. (2014). Role of SAGA in the asymmetric segregation of DNA circles during yeast ageing. eLife *3*.
50. Caudron, F., and Barral, Y. (2009). Septins and the lateral compartmentalization of eukaryotic membranes. Developmental cell *16*, 493-506.
51. Hu, Q., Milenkovic, L., Jin, H., Scott, M.P., Nachury, M.V., Spiliotis, E.T., and Nelson, W.J. (2010). A septin diffusion barrier at the base of the primary cilium maintains ciliary membrane protein distribution. Science *329*, 436-439.
52. Ewers, H., Tada, T., Petersen, J.D., Racz, B., Sheng, M., and Choquet, D. (2014). A Septin-Dependent Diffusion Barrier at Dendritic Spine Necks. PloS one *9*, e113916.

## FIGURE LEGENDS

**Figure 1. Age-dependent deposits associate with the endoplasmic reticulum.** (A) Representative 3D projected image of a cell expressing Sec61-GFP and Hsp104-mCherry. (B) The percentages of age-associated protein deposits (Hsp104-mCherry focus) in contact with different organelles (N=18-51/group). (C) Time-lapse imaging of budding cell expressing Hsp104-mCherry and Sec61-GFP. Arrowhead: deposit surrounded by an ER extension. (D) Quantification of the apposition of Hsp104-mCherry labeled deposits to the ER (Sec71-GFP), vacuole (Ym018c-GFP) and mitochondria (Tom70-GFP) during cell division. Images were acquired every 10 minutes over 100 minutes. 0 min time point is set at G1 (N=15/each). (E) Design of the mating experiments. (F) Time-lapse images at indicated time points after conjugaison. *MAT*a cell expresses Hsp104-mCherry (arrowhead: deposit) and Sec71-GFP (ER membrane marker); *Mat*α cell expresses Hsp104-mCherry; or (G) Yml018c-GFP (vacuolar membrane). (H) Quantification of apposition between labeled deposit (Hsp104-mCherry) and the ER (Sec71-GFP) or vacuole (Ymo018c) starting from first frame before fusion. (I-J) Single plane SIM images of cells expressing Sec71-GFP and Hsp104-mCherry.

Arrowheads: deposits at the nuclear envelope (I), and inside the nucleus (J). Scale bars (A) 2μm, (C, F-G) 5μm and (I-J) 1μm. See also Figures S1-S2.

**Figure 2. Localization to the ER membrane promotes the singularity of age-associated deposits.** (A) Time-lapse imaging of Hsp104-GFP in a middle-age mother cell (12-15 generations). Arrowheads: pre-existing age-associated deposit (red) and transient appearance of a second one (blue). (B-G) Time-lapse microscopy of a *MATa* cell expressing Hsp104-GFP (*Mat*a) fusing with a *MAT*α cell expressing Hsp104-mCherry. The experimental principles (B) and the fluorescence intensity profiles of representative 3D projected images are depicted. 0 min corresponds to time of cell-cell fusion. (H) Deletion of *PRM3* impairs nuclear and ER fusion [50]. (I-J) Representative images at indicated time points after fusion (I) of wild type zygotes and (J) *prm3Δ/prm3Δ* mutant zygotes expressing Hsp104-mCherry (grey) and Pre6-GFP (blue, nucleus). (K-L) Quantification of wild type and *prm3Δ/prm3Δ* mutant zygotes fusing deposits before completing their first division. Graph displays mean in % ±SEM, (N=42-81). Scale bars: 5μm. See also Figure S3 and Movie S1.

**Figure 3. Lateral diffusion barriers at the endoplasmic reticulum inhibit deposit formation in the daughter cells.** (A) Representative projections of wild type, *bud1Δ*, *bud6Δ* and *sur2Δ* mutant cells expressing Hsp104-GFP (grey) imaged 285 min. apart. Red Arrowheads: deposit in the aged mother cell (red) and deposits appearing in the daughter cells (blue). (B) Percentage of divisions in which the deposit passes to the daughter cells (from aged mother cell with a single deposit) in strains of indicated genotype (N=117-269). (C) Percentage of daughter cells forming a stable deposit during their first cell cycle as in B (N=82-244). The graphs display mean ±SEM. Scale bars 5μm. See also Figure S4.

**Figure 4. ER coupling of farnesylated Ydj1 and the diffusion barriers in confining protein deposit formation to the mother cell.** (A-B) Representative projections of wild type and *Ydj1-C406S* mutant cells imaged 120 min apart as in Fig. 3A. Arrowheads: deposits of

the mother cell (red) and deposits appearing in the daughter cells (blue). M=mother, D=daughter, GD=granddaughter cell. (C) Percentage of divisions with deposit passing from the mother cell into her daughter. (N=217-502). (D) Percentage of daughter cells forming a stable deposit during their first division cycle (as in 1C; N=318-343). (E) Representative images of *YDJ1-C406S sur2Δ, YDJ1-C406S bud1Δ and YDJ1-C406S bud6Δ* double mutant cells as in A. (F) Percentage of daughter cells forming a deposit during their first division cycle (N=256-343). Scale bars: 5μm, graphs display mean ±SEM. See also Figure S5.

**Figure 5. Ydj1 is compartmentalized by ER-tethering and diffusion barriers and suppresses the Sup35 prion phenotype.** (A) Sketch of the experimental design. (B,C) Quantification of the diffusion coefficient (in log scale) in the indicated compartments (A) or presented as a mother/bud ratio (C) of GFP (N=53), Ydj1-GFP$^{FS}$ (N=149), Ydj1-GFP$^{C406S}$ (N=48), and Ydj1-GFP$^{FS}$ in *sur2Δ* cells (N=98). (D) Schematic representation of the FLIP assay: GFP-Ydj1 was continuously photobleached in the mother domain and the fluorescence decay was measured over time in mother (red) and bud (orange). (E) Average FLIP curves of GFP-Ydj1 (upper panel) (N=40); Ydj1-GFP (lower panel) (N=39). (F) Barrier Index for the indicated markers in cells of indicated genotypes. (G) Schematic representation of the effects of Sup35 in translation termination in its non-prion [*psi*-], weak and strong prion [*PSI*+] states. (H) Fluorescence intensity measured by flow cytometer of *YDJ1*, *YDJ1-C406S* and *Ydj1-L135S* cells in the [*PSI*+] and [*psi*-] states. Graphs display mean ±SEM.

**Movie S1. Age-associated protein deposits derived from mating partners merge together after cell-cell fusion.** The fate of age-associated protein deposits were followed as they enter the same cellular milieu by imaging haploid cells of the opposite mating type expressing either Hsp104-GFP or Hsp104-mCherry before and after they mate to form a diploid. Time frame is 10 minutes. Related to Figure 2.

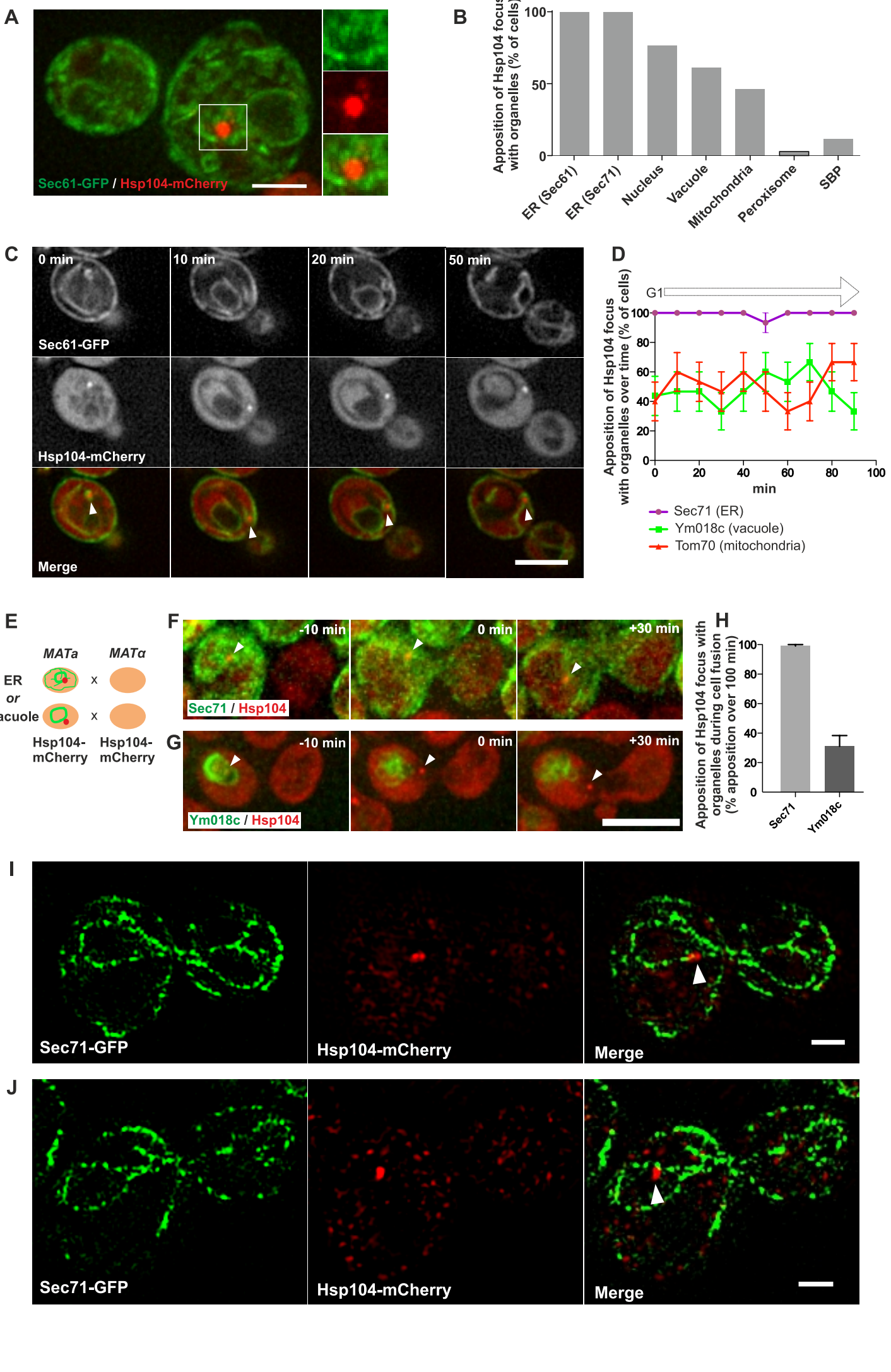
A
Sec61-GFP / Hsp104-mCherry
B
Apposition of Hsp104 focus with organelles (% of cells)
100
50
0
ER (Sec61)
ER (Sec71)
Nucleus
Vacuole
Mitochondria
Peroxisome
SBP
C
0 min
10 min
20 min
50 min
Sec61-GFP
Hsp104-mCherry
Merge
D
Apposition of Hsp104 focus with organelles over time (% of cells)
G1
100
80
60
40
20
0
0
20
40
60
80
100
min
Sec71 (ER)
Ym018c (vacuole)
Tom70 (mitochondria)
E
MATa
MATα
ER
or
Vacuole
x
x
Hsp104-mCherry
Hsp104-mCherry
F
-10 min
0 min
+30 min
Sec71 / Hsp104
G
-10 min
0 min
+30 min
Ym018c / Hsp104
H
Apposition of Hsp104 focus with organelles during cell fusion (% apposition over 100 min)
100
80
60
40
20
0
Sec71
Ym018c
I
Sec71-GFP
Hsp104-mCherry
Merge
J
Sec71-GFP
Hsp104-mCherry
Merge

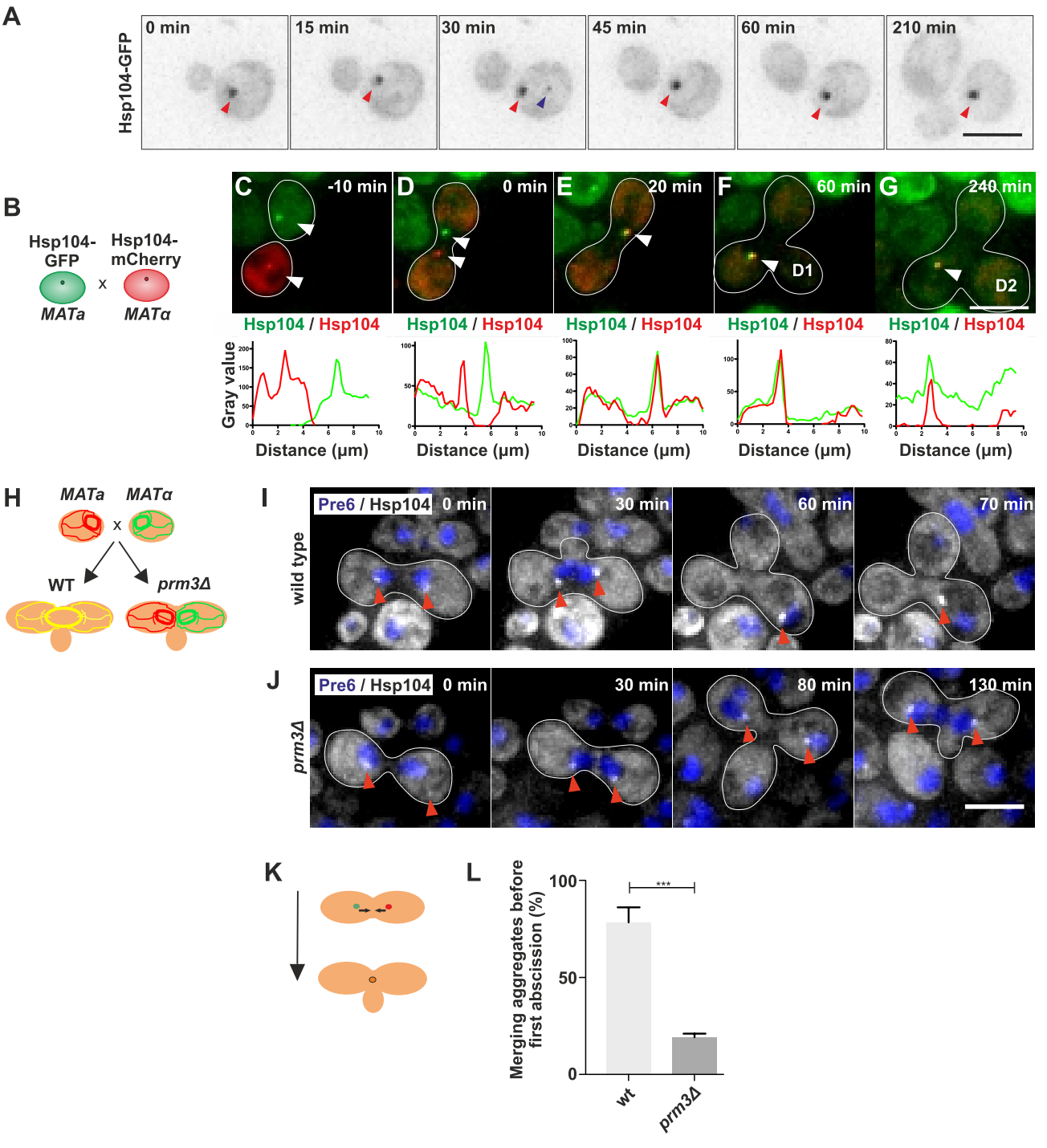
A
Hsp104-GFP
0 min
15 min
30 min
45 min
60 min
210 min
B
Hsp104-GFP
Hsp104-mCherry
MATa
MATα
C -10 min
D 0 min
E 20 min
F 60 min
G 240 min
D1
D2
Hsp104 / Hsp104
Gray value
Distance (μm)
H
MATa
MATα
WT
prm3Δ
I
wild type
Pre6 / Hsp104
0 min
30 min
60 min
70 min
J
prm3Δ
Pre6 / Hsp104
0 min
30 min
80 min
130 min
K
L
Merging aggregates before first abscission (%)
100
50
0
***
wt
prm3Δ

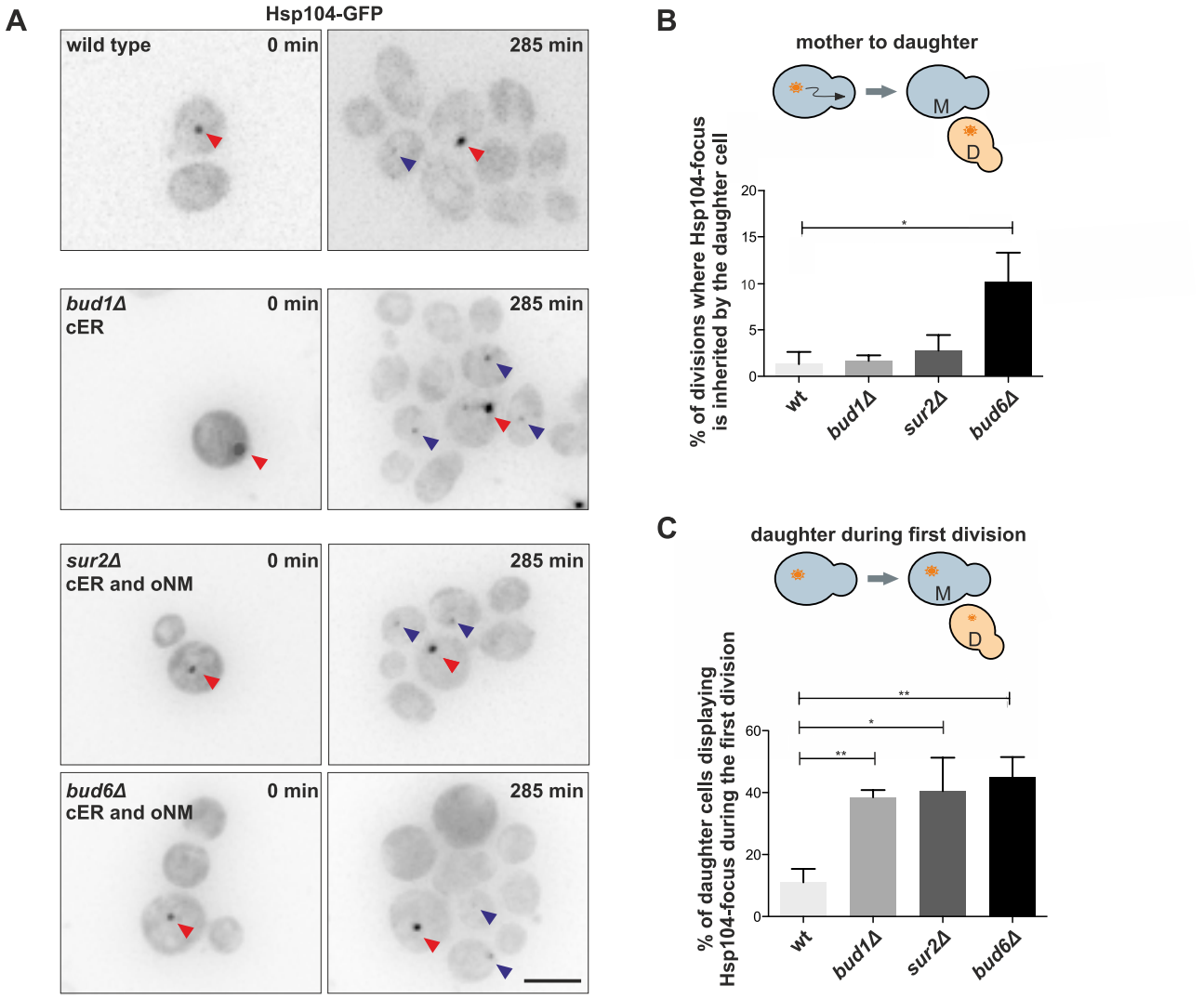
A
Hsp104-GFP
wild type
0 min
285 min
bud1Δ
cER
0 min
285 min
sur2Δ
cER and oNM
0 min
285 min
bud6Δ
cER and oNM
0 min
285 min
B
mother to daughter
M
D
% of divisions where Hsp104-focus is inherited by the daughter cell
20
15
10
5
0
*
wt
bud1Δ
sur2Δ
bud6Δ
C
daughter during first division
M
D
% of daughter cells displaying Hsp104-focus during the first division
60
40
20
0
**
*
**
wt
bud1Δ
sur2Δ
bud6Δ

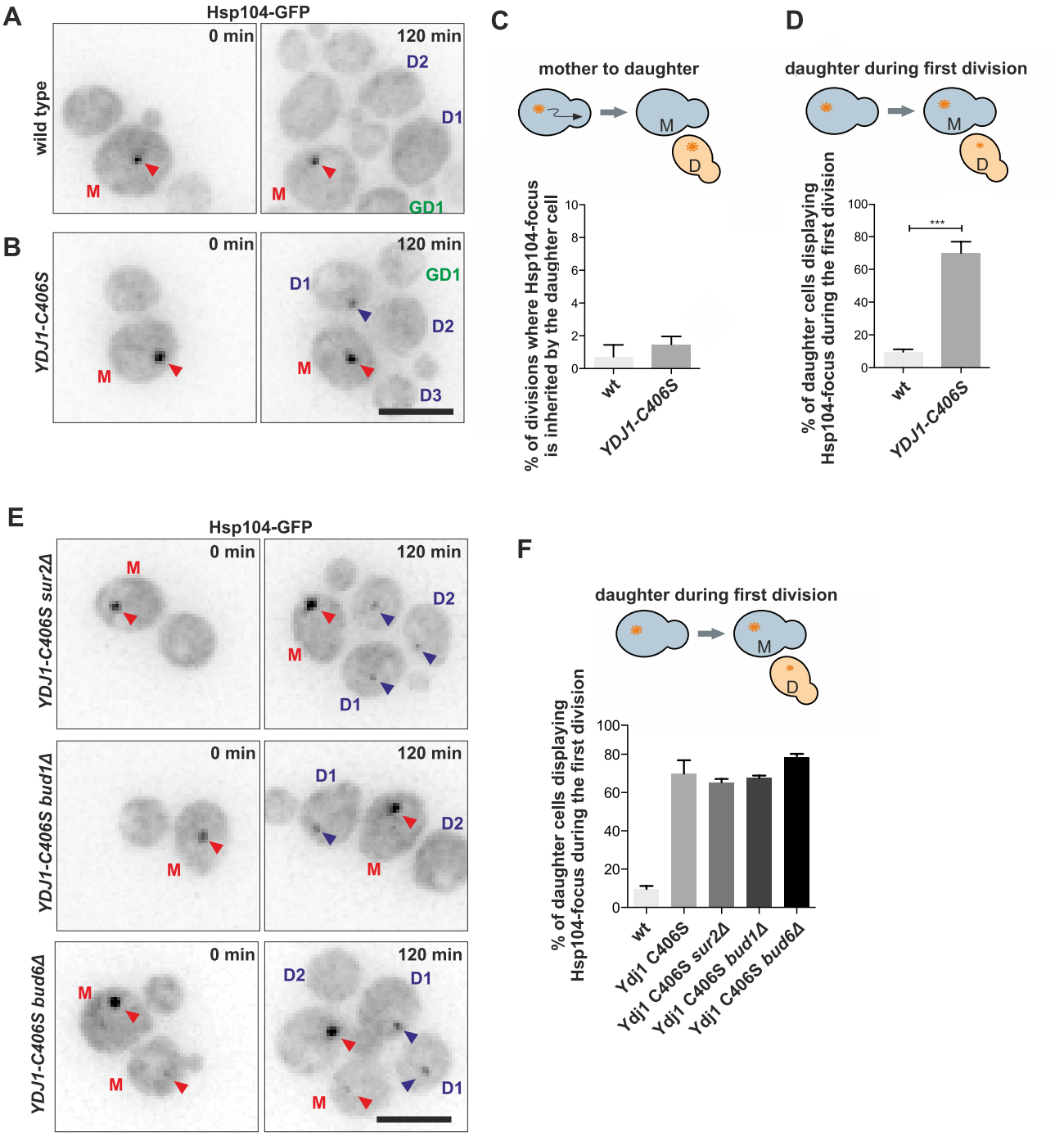
A
Hsp104-GFP
wild type
0 min
120 min
M
D2
D1
GD1
B
YDJ1-C406S
D3
C
mother to daughter
D
% of divisions where Hsp104-focus is inherited by the daughter cell
wt
YDJ1-C406S
daughter during first division
% of daughter cells displaying Hsp104-focus during the first division
***
E
YDJ1-C406S sur2Δ
YDJ1-C406S bud1Δ
YDJ1-C406S bud6Δ
F
Ydj1 C406S
Ydj1 C406S sur2Δ
Ydj1 C406S bud1Δ
Ydj1 C406S bud6Δ

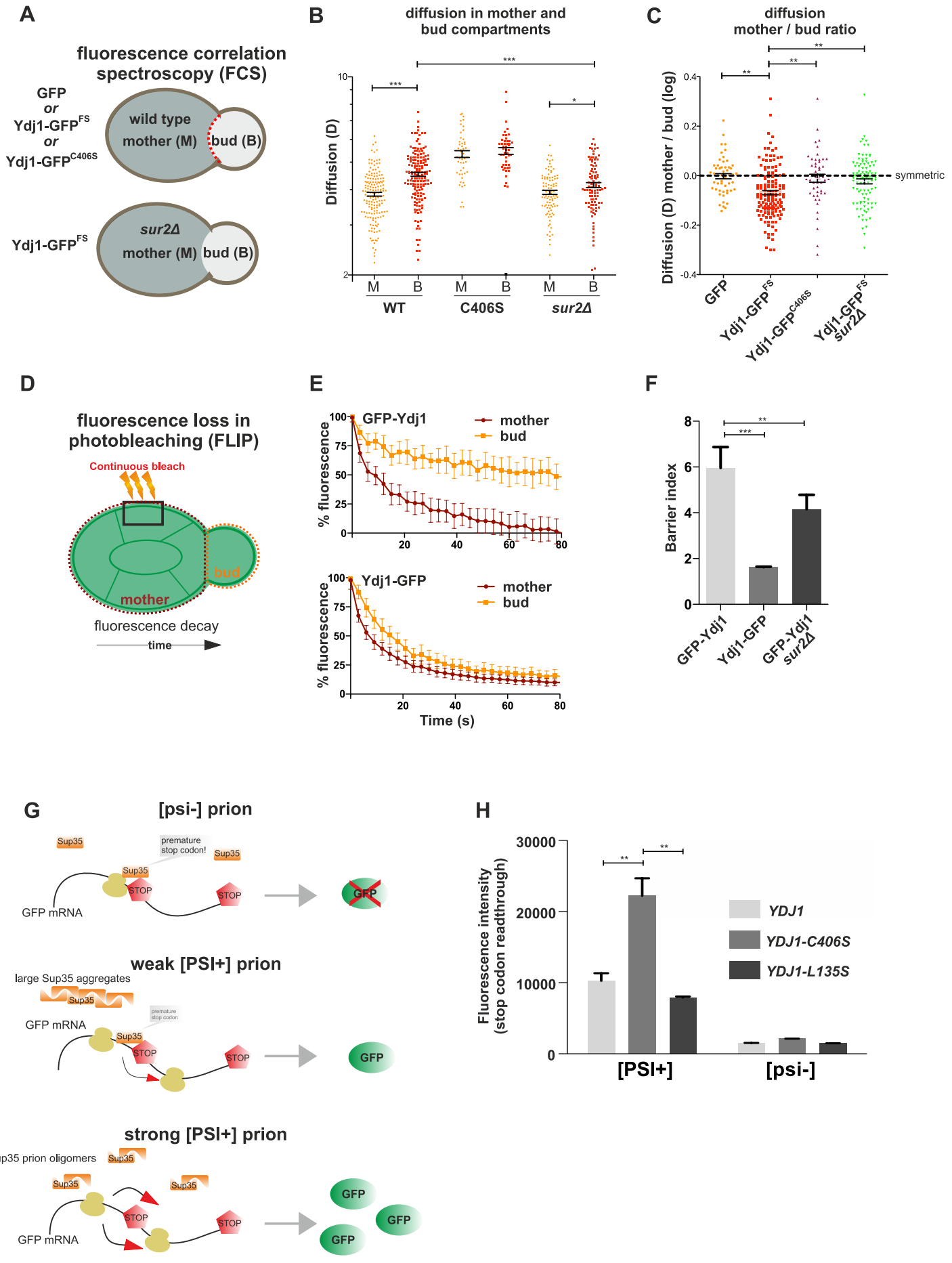
A
fluorescence correlation spectroscopy (FCS)
GFP
or
Ydj1-GFP^FS
or
Ydj1-GFP^C406S
wild type
mother (M)
bud (B)
Ydj1-GFP^FS
sur2Δ
mother (M)
bud (B)
B
diffusion in mother and bud compartments
Diffusion (D)
M
B
WT
C406S
sur2Δ
C
diffusion mother / bud ratio
Diffusion (D) mother / bud (log)
symmetric
GFP
Ydj1-GFP^FS
Ydj1-GFP^C406S
Ydj1-GFP^FS sur2Δ
D
fluorescence loss in photobleaching (FLIP)
Continuous bleach
bud
mother
fluorescence decay
time
E
GFP-Ydj1
mother
bud
% fluorescence
Ydj1-GFP
Time (s)
F
Barrier index
GFP-Ydj1
Ydj1-GFP
GFP-Ydj1 sur2Δ
G
[psi-] prion
Sup35
premature stop codon!
STOP
GFP mRNA
GFP
weak [PSI+] prion
large Sup35 aggregates
strong [PSI+] prion
Sup35 prion oligomers
H
Fluorescence intensity (stop codon readthrough)
YDJ1
YDJ1-C406S
YDJ1-L135S
[PSI+]
[psi-]

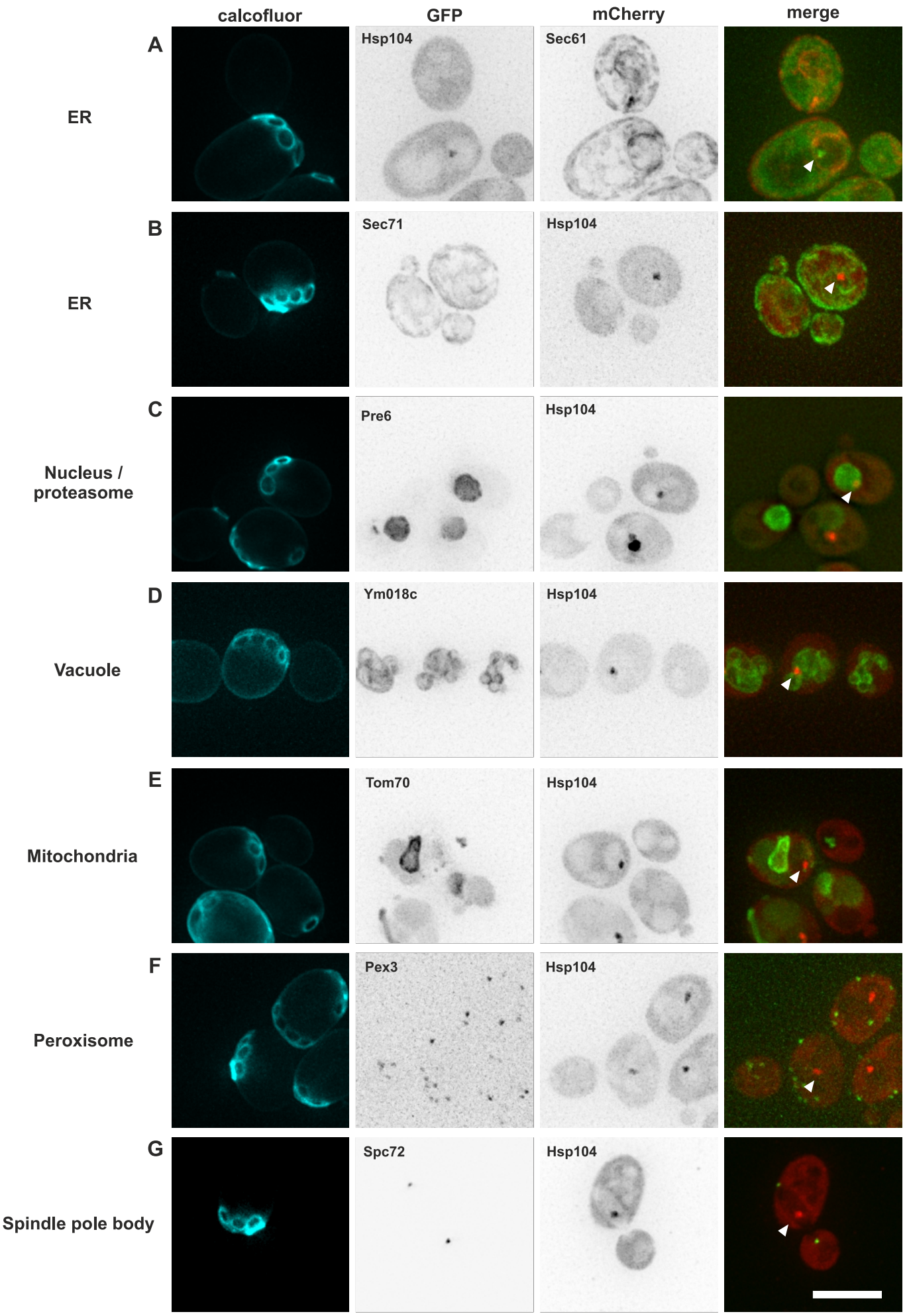


**Supplemental Figure 1, Relates to Figure 1. Localization of age-associated deposits in respect to organelles.** Representative z-projected images of age-associated protein deposits in 3-6 generation old cells expressing (A) Hsp104-GFP and Sec61-mCherry (ER); (B) Hsp104-mCherry and Sec71-GFP (ER); (C) Pre6-GFP (nucleus/proteasome); (D) Yml018C-GFP (vacuolar membrane); (E) Tom-70-GFP (mitochondria); (F) Pex3-GFP (peroxisome) and (G) Spc72-GFP (spindle pole bodies). Scale bar: 5μm.

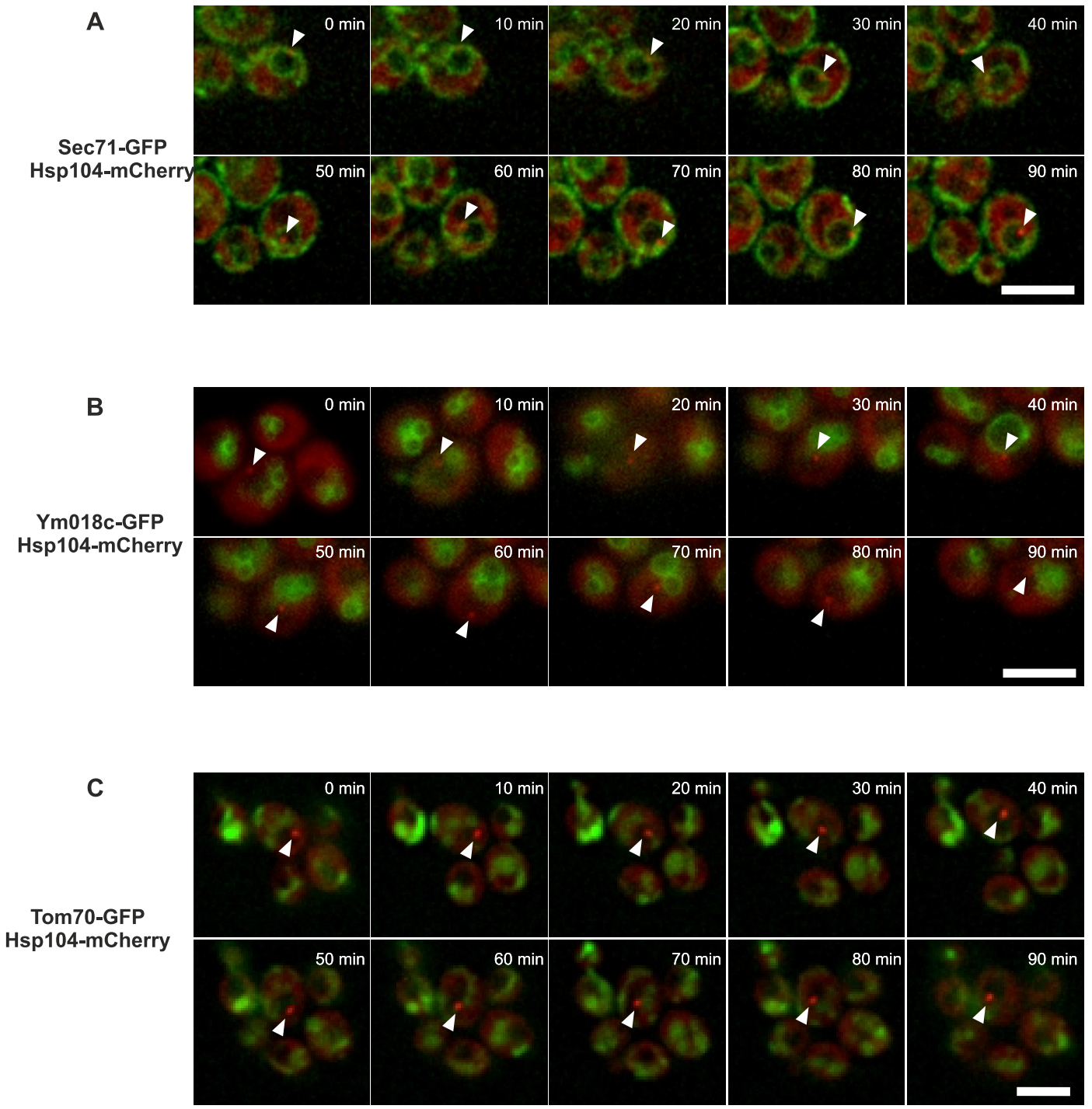


**Supplemental Figure 2, Relates to Figure 1. Time lapse analysis of the apposition of Hsp104-labelled deposits with organelles.** Individual frames corresponding to the focal plane of the deposit over the course of a cell division of (A) Hsp104-mCherry and Sec71-GFP; (B) Hsp104-mCherry and Ym018c-GFP and (C) Hsp104-mCherry and Tom70-GFP. Scale bars: 5μm.

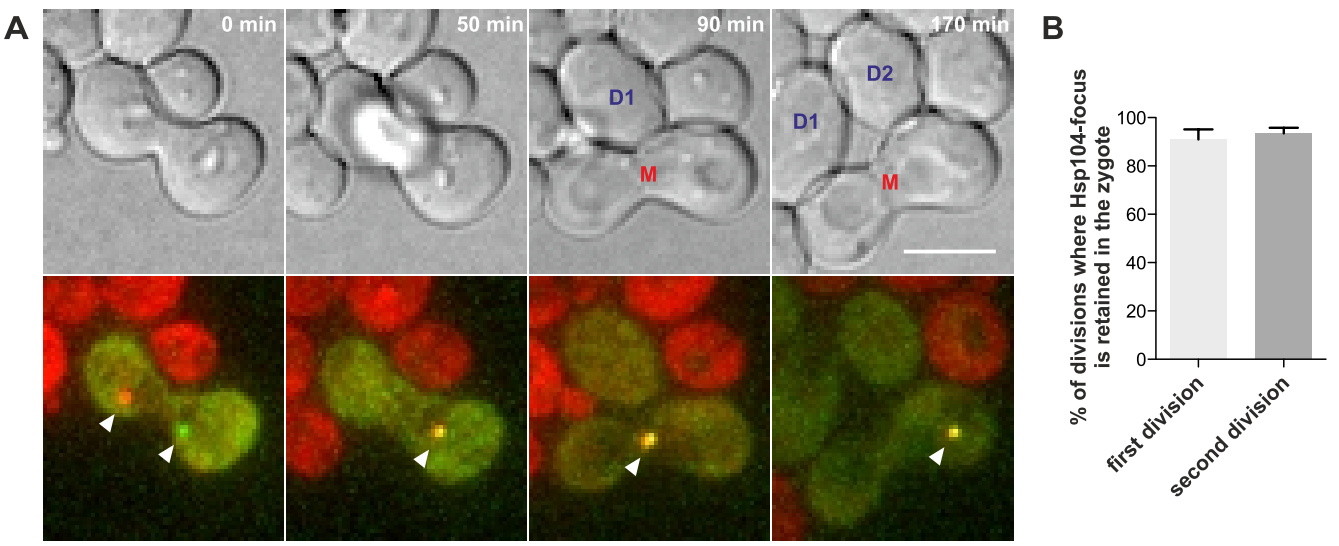


**Supplemental Figure 3, Relates to Figure 2. Age-associated deposits are retained in the zygote during cell division.** (A) Time lapse images of age-associated protein deposits (arrowheads) in a newly formed zygote. M = zygote, D1 and D2, daughter cells. (B) Percentages of zygotic divisions where the deposit is retained during the first and second division. (N=130-180). Graph displays ±SEM. Scale bar: 5µm.

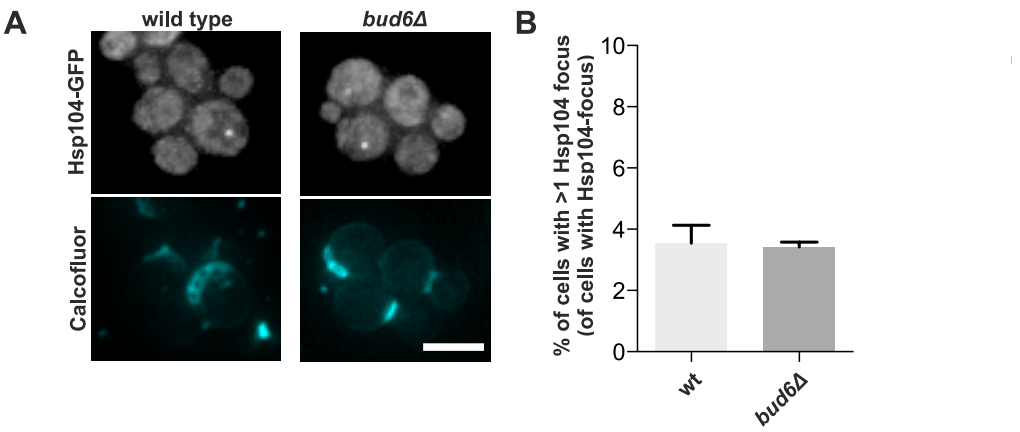


**Supplemental Figure 4, Relates to Figure 3. Downregulation of the diffusion barriers does not lead to deposit fragmentation.** (A) Representative images of wild type and *bud6Δ* cells expressing Hsp104-GFP (upper panel) and stained with calcofluor (lower panel). (B) Quantification of the percentage of cells displaying ≥2 deposits per cell (of all deposit containing cells). (N=201-348 from three biological replicates). Graph displays mean ±SEM. Scale bar: 5µm.

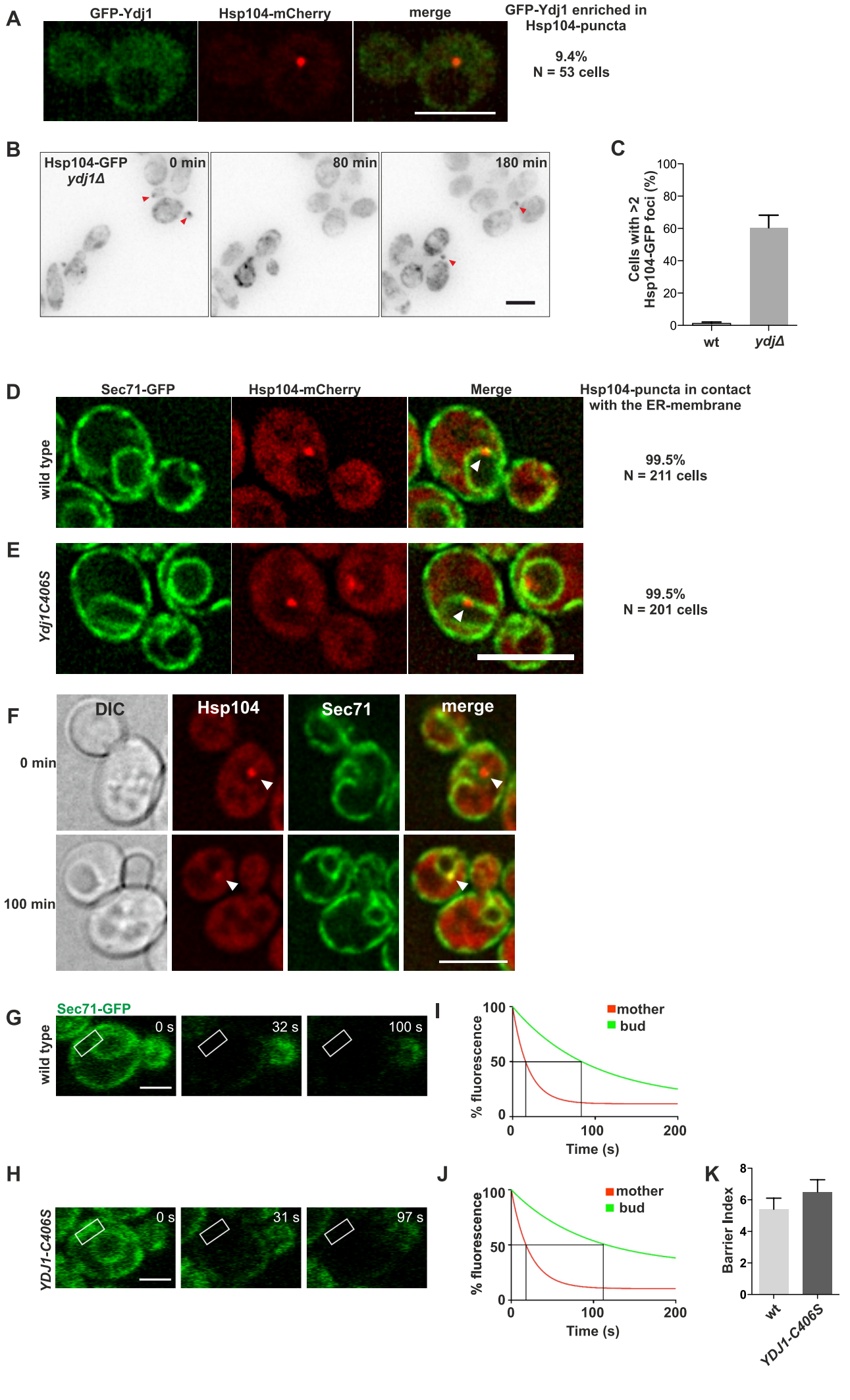
A
GFP-Ydj1
Hsp104-mCherry
merge
GFP-Ydj1 enriched in Hsp104-puncta
9.4%
N = 53 cells
B
Hsp104-GFP
ydj1Δ
0 min
80 min
180 min
C
Cells with >2 Hsp104-GFP foci (%)
100
80
60
40
20
0
wt
ydjΔ
D
Sec71-GFP
Hsp104-mCherry
Merge
Hsp104-puncta in contact with the ER-membrane
wild type
99.5%
N = 211 cells
E
Ydj1C406S
99.5%
N = 201 cells
F
DIC
Hsp104
Sec71
merge
0 min
100 min
G
Sec71-GFP
wild type
0 s
32 s
100 s
I
mother
bud
% fluorescence
100
50
0
0
100
200
Time (s)
H
YDJ1-C406S
0 s
31 s
97 s
J
mother
bud
% fluorescence
100
50
0
0
100
200
Time (s)
K
Barrier Index
8
6
4
2
0
wt
YDJ1-C406S

**Supplemental Figure 5, Relates to Figure 4. *YDJ1C406S* mutant cells do not display a barrier defect or obvious disengagement of deposits form the ER membrane.** (A) Representative aged mother cell expressing GFP-Ydj1 and Hsp104-mCherry. (B) Representative time-frame images from Hsp104-GFP expressing *ydj1Δ* mutant cells. Arrowheads indicate small deposits entering the bud. (C) Percentage of cells displaying >2 Hsp104 foci N=2 (wt); 3(*ydj1Δ*), 87-251 cells per group. (D-E) Representative images of wild type (D) and *Ydj1-C406S* (E) cells expressing Sec71-GFP and Hsp104-mCherry. (F) Representative time-lapse frames of *YDJ1-C406S* cells expressing Sec71-GFP and Hsp104-mCherry prior to (left) and after (right) the formation of Hsp104-deposit in the daughter cell. (G-H) Representative time frames from the FLIP analysis of Sec71-GFP in wild type and Ydj1C406S mutant cells. (I-J) Fluorescence decay over time for the wild type (I) and Ydj1C406S (J) are shown. (K) Graph shows Barrier index (BI), indicating the time of 50% fluorescence loss in bud compartment divided by the time of 50% fluorescence loss in mother compartment. Total of 60 cells were analysed per genotype. Mean ± SD. Scale bars: 5μm (A-G; D-F), 2 μm (G-H).

**SUPPLEMENTAL EXPERIMENTAL PROCEDURES**

**Yeast strains**

Yeast strains were generated as described in [S1] and are listed below.

| Strain | Genotype |
|---|---|
| 5644 | ade2::hisG his3 leu2 lys2 ura3D0 trp1D63 hoD::SCW11pr-Cre-EBD78-NatMX loxP-UBC9-loxP-LEU2 loxP-CDC20-Intron-loxP-HPHMX Hsp104-GFP:HIS3 |
| 5658 | ade2::hisG his3 leu2 met15D::ADE2 ura3D0 trp1D63 hoD::SCW11pr-Cre-EBD78-NatMX loxP-UBC9-loxP-LEU2 loxP-CDC20-Intron-loxP-HPHMX Hsp104-mCherry:KanMX |
| 5683 | ade2::hisG his3 leu2 met15D::ADE2 ura3D0 trp1D63 hoD::SCW11pr-Cre-EBD78-NatMX loxP-UBC9-loxP-LEU2 loxP-CDC20-Intron-loxP-HPHMX Hsp104-Cherry:KanMX SPC72-GFP:HIS3 |
| 5761 | ade2::hisG his3 leu2 lys2 ura3D0 trp1D63 hoD::SCW11pr-Cre-EBD78-NatMX loxP-UBC9-loxP-LEU2 loxP-CDC20-Intron-loxP-HPHMX sur2::kanMX Hsp104-GFP:HIS3 |
| 5781 | ade2::hisG his3 leu2 met15D::ADE2 ura3D0 trp1D63 hoD::SCW11pr-Cre-EBD78-NatMX loxP-UBC9-loxP-LEU2 loxP-CDC20-Intron-loxP-HPHMX Hsp104-Cherry:KanMX Sec61-GFP:HIS3 |
| 5791 | ade2::hisG his3 leu2 lys2 ura3D0 trp1D63 hoD::SCW11pr-Cre-EBD78-NatMX loxP-UBC9-loxP-LEU2 loxP-CDC20-Intron-loxP-HPHMX bud6::kanMX Hsp104-GFP:HIS3 |
| 5792 | ade2::hisG his3 leu2 lys2 ura3D0 trp1D63 hoD::SCW11pr-Cre-EBD78-NatMX loxP-UBC9-loxP-LEU2 loxP-CDC20-Intron-loxP-HPHMX bud1::kanMX Hsp104-GFP:HIS3 |
| 5812 | ade2::hisG his3 leu2 met15D::ADE2 ura3D0 trp1D63 hoD::SCW11pr-Cre-EBD78-NatMX loxP-UBC9-loxP-LEU2 loxP-CDC20-Intron-loxP-HPHMX Pre6-GFP:HIS3 Hsp104-Cherry:KanMX |
| 5840 | YML018C-GFP:HIS3 HSP104-Cherry:KanMX ade2::hisG his3 leu2 met15D::ADE2 ura3D0 trp1D63 hoD::SCW11pr-Cre-EBD78-NatMX loxP-UBC9-loxP-LEU2 loxP-CDC20-Intron-loxP-HPHMX |
| 6617 | MATa his3D1 leu2D0 met15D0 ura3D0 Ydj1-GFP:HIS |
| 11533 | MATa his3D1 leu2D0 met15D0 ura3D0 Pre6-GFP:HIS Hsp104-mCherry:KanMX |
| 11534 | MATalpha his3D1 leu2D0 met15D0 ura3D0 Pre6-GFP:HIS Hsp104-Cherry:KanMX |
| 11535 | MATa his3D1 leu2D0 met15D0 ura3D0 Pre6-GFP:HIS Hsp104-Cherry:KanMX pre3::NatMX |
| 11536 | MATalpha his3D1 leu2D0 met15D0 ura3D0 Pre6-GFP:HIS Hsp104-Cherry:KanMX prm3::NatMX |
| 11538 | ade2::hisG his3 leu2 lys2 ura3D0 trp1D63 hoD::SCW11pr-Cre-EBD78-NatMX loxP-UBC9-loxP-LEU2 loxP-CDC20-Intron-loxP-HPHMX Tom70-GFP:HIS3 Hsp104-mCherry:KanMX |
| 11539 | ade2::hisG his3 leu2 lys2 ura3D0 trp1D63 hoD::SCW11pr-Cre-EBD78-NatMX loxP-UBC9-loxP-LEU2 loxP-CDC20-Intron-loxP-HPHMX Pex3-GFP:HIS3 Hsp104-mCherry:KanMX |
| 13352 | ura3-52 his3Δ200 leu2 lys2-801 trp1Δ63, MET15 Sec71-GFP:HIS3 Hsp104-mCherry:KAnMX |
| 13353 | ade2::hisG his3 leu2 met15D::ADE2 ura3D0 trp1D63 hoD::SCW11pr-Cre-EBD78-NatMX loxP-UBC9-loxP-LEU2 loxP-CDC20-Intron-loxP-HPHMX Ydj1C406S:TRP Hsp104-GFP:HIS3 |

| | |
|---|---|
| 13459 | ade2::hisG his3 leu2 met15D::ADE2 ura3D0 trp1D63 hoD::SCW11pr-Cre-EBD78-NatMX loxP-UBC9-loxP-LEU2 loxP-CDC20-Intron-loxP-HPHMX Ydj1C406S:TRP sur2::KanMX Hsp104-GFP:HIS3 |
| 13460 | ade2::hisG his3 leu2 met15D::ADE2 ura3D0 trp1D63 hoD::SCW11pr-Cre-EBD78-NatMX loxP-UBC9-loxP-LEU2 loxP-CDC20-Intron-loxP-HPHMX Ydj1C406S:TRP bud6::KanMX Hsp104-GFP:HIS3 |
| 13554 | ade2::hisG his3 leu2 met15D::ADE2 ura3D0 trp1D63 hoD::SCW11pr-Cre-EBD78-NatMX loxP-UBC9-loxP-LEU2 loxP-CDC20-Intron-loxP-HPHMX Ydj1_C406S_TRP Sec71-GFP:HIS3 Hsp104-mCherryKanMX |
| 13555 | ade2::hisG his3 leu2 met15D::ADE2 ura3D0 trp1D63 hoD::SCW11pr-Cre-EBD78-NatMX loxP-UBC9-loxP-LEU2 loxP-CDC20-Intron-loxP-HPHMX Sec71-GFP:HIS3 Hsp104-mCherryKanMX |
| 13729 | his3Δ1 leu2Δ0 met15Δ0 ura3Δ0 Ydj1-GFP-FS:HIS3 |
| 13775 | ade2::hisG his3 leu2 met15D::ADE2 ura3D0 trp1D63 hoD::SCW11pr-Cre-EBD78-NatMX loxP-UBC9-loxP-LEU2 loxP-CDC20-Intron-loxP-HPHMX Ydj1_C406S:TRP Bud6::KAnMX Ydj1::C406S:TRP Hsp104-GFP:HIS3 |
| 13776 | his3Δ1 leu2Δ0 ura3Δ0 met15Δ0 Sec61-mCherry:KanMX Hsp104-GFP:HIS3 |
| 14009 | his3Δ1 leu2Δ0 met15Δ0 ura3Δ0 Ydj1-GFP-FS:HIS3 Ydj1-GFP-FS:HIS3 sur2::NatMX |
| 14010 | leu2Δ0 met15Δ0 ura3Δ0 S.cer_CYC1ter-hph_dN-SceI-URA3pr-URA3-URA3ter-S.par_NOP1pr-sfGFP-Ydj1 |
| 14011 | leu2Δ0 met15Δ0 ura3Δ0 S.cer_CYC1ter-hph_dN-SceI-URA3pr-URA3-URA3ter-S.par_NOP1pr-sfGFP-Ydj1 sur2::HygMX |
| 14015 | leu2-3,-112; his3-11,-15; trp1-1; ura3-1; ade1-4; can1-100, Ydj1::KanMX +pRS304 pGPD GST-UGA-GFP-pest:URA3 pRS315 Ydj1:LEU [RNQ+] [PSI+] |
| 14016 | leu2-3,-112; his3-11,-15; trp1-1; ura3-1; ade1-4; can1-100, Ydj1::KanMX +pRS304 pGPD GST-UGA-GFP-pest:URA3 pRS315 Ydj1:LEU [RNQ+] [psi-] |
| 14017 | leu2-3,-112; his3-11,-15; trp1-1; ura3-1; ade1-4; can1-100, Ydj1::KanMX +pRS304 pGPD GST-UGA-GFP-pest:URA3 pRS315 Ydj1-C406S:LEU [RNQ+] [PSI+] |
| 14018 | leu2-3,-112; his3-11,-15; trp1-1; ura3-1; ade1-4; can1-100, Ydj1::KanMX +pRS304 pGPD GST-UGA-GFP-pest:URA3 pRS315 Ydj1-C406S:LEU [RNQ+] [psi-] |
| 14019 | leu2-3,-112; his3-11,-15; trp1-1; ura3-1; ade1-4; can1-100, Ydj1::KanMX +pRS304 pGPD GST-UGA-GFP-pest:URA3 pRS315 Ydj1-L135S:LEU [RNQ+] [PSI+] |
| 14020 | leu2-3,-112; his3-11,-15; trp1-1; ura3-1; ade1-4; can1-100, Ydj1::KanMX +pRS304 pGPD GST-UGA-GFP-pest:URA3 pRS315 Ydj1-L135:LEU [RNQ+] [psi-] |
| M. Aldea | his3Δ1 leu2Δ0 met15Δ0 ura3Δ0 YDJ1-GFP-FS-C406S::HIS3 |
| M. Aldea | his3Δ1 leu2Δ0 met15Δ0 ura3Δ0 TEFp-GFP-NatN2::ura3-0 |

For the Ydj1 mutagenesis, *TRP1* gene was PCR amplified using oligonucleotides that contained a (1217 G->C) substitution in the overhang *YDJ1*-targeting sequence to change the cysteine 406 into serine. The cassette amplification and transformation into yeast cells was done as described in [S2] and the correct targeting was validated by sequencing.

**Cell culturing and preparation**

For imaging, cells were cultured at 30ºC in YPD media and prepared for imaging (performed in synthetic complete media) as described in [1]. For the mating experiments, cells ($1.85x10^7$) of opposite mating types were centrifuged 500g for 5 minutes and re-suspended in 40 µl SC media, mixed and immediately imaged with 10min intervals. To obtain aged cells, cells were biotinylated with Sulfo-NHS-LC biotin (Pierce), grown for the desired period in YPD, incubated with uMACS Streptavidin microbeads (Miltenyi Biotec) and affinity purified with the MACS separation column. For aging periods >8 hrs, the mother enrichment program was used [S3]. For analysis of replicative age, bud scars were stained with 5 µg/ml Calcofluor White (Fluorescece Brightner 28, F3543, Sigma). For structured illumination microscopy, cells were fixed in 4 % paraformaldehyde for 15 min, washed

once in 100mM potassium phosphate buffer containing 1,2M sorbitol and stored in this buffer in a light-sealed environment at 4ºC. Prior to imaging, cells were placed in Vectashield antifade mounting media (H1000, Vector), mounted between a #1.5 high precision coverslip (Marienfeld Superior) and an objective slide and (Marienfeld Superior) and sealed with nail polish.

FLIP experiment was performed as described in [S4, S5]. Briefly, cells were grown at 30°C on YPD for 12-16 hours prior to imaging, and immobilized on a 2% agar pad containing synthetic non-fluorescent medium.

**Image analyses**

All image analyses were performed with Image J (Fiji) software as described in [S1]. The quantification of age-associated deposit (Hsp104-labelled focus) inheritance in Figures 1 and 4 was performed form mother cells with a single deposit that were imaged every 10-15 minutes. For appearance of deposits in the daughter cells, only those cells that were born without a deposit but formed an deposit that was present until the completion of the first division were counted. The co-localization with the organelles was quantified by examining all the z-planes where the deposit (bright Hsp104 focus) was detected. Deposits that displayed overlapping or adjacent localization with the organelle markers were scored as co-localizing structures.

For the FLIP quantification, the total integrated fluorescent density in the entire the mother and bud was quantified. After subtracting background, the fluorescent signal of the mother and bud were normalized to the mean of five neighboring control cells and set to 100% at the beginning of the experiment. All experiments were pooled and analyzed using Prism 5b to fit a one-phase decay curve constraining the first bleaching point to 100%. The barrier index was defined as the ratio of the times needed to lose 50% of the initial fluorescent signal in the bud over the mother compartment.

**Fluorescence correlation spectroscopy**

Quantitative analysis of Ydj1-GFP diffusion by FCS was performed essentially as described [S6]. Specifically, cells were prebleached to attain count rates within the 100-500 kHz range during acquisition for periods of 5 sec. Correlation data were fitted in the 10 µsec to 100 msec range of time intervals with the aid of ImageJ plugins developed by Jay Unruh (Stowers Institute for Medical Research, Kansas City, MO) to obtain diffusion coefficients. Duplicate measurements were always taken and outliers were removed from analysis if the relative standard error of the fitted coefficient of diffusion was higher than 50%, or the fitted autocorrelation intersect was higher than 1.01 as a result of strong perturbations in the average count rate during acquisition.

**Flow cytometry**

For the stop codon read through experiments, *ydj1Δ* [*PSI*+] and [*psi*-] cells expressing PRS315- *YDJ1*, *YDJ1-C406S* or *YDJ1-L135S* [S7] and chromosomally integrated pGPD GST-UGA-GFP-pest [S8] were grown in SC-leu media. The GFP fluorescence intensity was measured with a BD Accuri C6 Flow Cytometer using 488 nm laser and 533/30 BD filter for 100 000 cells/ clone (3 clones each). The data was analyzed using FlowJo software (FlowJo LLC).

**SUPPLEMENTAL REFERENCES**


S1. Saarikangas, J., and Barral, Y. (2015). Protein aggregates are associated with replicative aging without compromising protein quality control. eLife *4*.

S2. Janke, C., Magiera, M.M., Rathfelder, N., Taxis, C., Reber, S., Maekawa, H., Moreno-Borchart, A., Doenges, G., Schwob, E., Schiebel, E., et al. (2004). A versatile toolbox for PCR-based tagging of yeast genes: new fluorescent proteins, more markers and promoter substitution cassettes. Yeast *21*, 947-962.

S3. Lindstrom, D.L., and Gottschling, D.E. (2009). The mother enrichment program: a genetic system for facile replicative life span analysis in Saccharomyces cerevisiae. Genetics *183*, 413-422, 411SI-413SI.

S4. Bolognesi, A., Sliwa-Gonzalez, A., Prasad, R., and Barral, Y. (2016). Fluorescence Recovery After Photo-Bleaching (FRAP) and Fluorescence Loss in Photo-Bleaching (FLIP) Experiments to Study Protein Dynamics During Budding Yeast Cell Division. Methods Mol Biol *1369*, 25-44.

S5. Clay, L., Caudron, F., Denoth-Lippuner, A., Boettcher, B., Buvelot Frei, S., Snapp, E.L., and Barral, Y. (2014). A sphingolipid-dependent diffusion barrier confines ER stress to the yeast mother cell. eLife *3*, e01883.

S6. Slaughter, B.D., Schwartz, J.W., and Li, R. (2007). Mapping dynamic protein interactions in MAP kinase signaling using live-cell fluorescence fluctuation spectroscopy and imaging. Proceedings of the National Academy of Sciences of the United States of America *104*, 20320-20325.

S7. Summers, D.W., Douglas, P.M., Ren, H.Y., and Cyr, D.M. (2009). The type I Hsp40 Ydj1 utilizes a farnesyl moiety and zinc finger-like region to suppress prion toxicity. J Biol Chem *284*, 3628-3639.
S8. Derdowski, A., Sindi, S.S., Klaips, C.L., DiSalvo, S., and Serio, T.R. (2010). A size threshold limits prion transmission and establishes phenotypic diversity. Science *330*, 680-683.